Journal of the European Ceramic Society **17** (1997) 1061–1082

PII: S0955-2219(96)00222-1
0955-2219/97/$17.00

Review: Structural Ceramic Nanocomposites

Martin Sternitzke*

University of Oxford, Department of Materials, Parks Road, Oxford OX1 3PH, UK

(Received and accepted 25 October 1996)

Abstract

Structural ceramic nanocomposites are reviewed with emphasis on the Al_2O_3/SiC and Si_3N_4/SiC systems. The incorporation of a nanosized second phase, such as SiC, into a ceramic matrix can lead to an improvement in mechanical properties. It is still unclear, however, whether those improvements can directly be related to an intrinsic 'nanocomposite effect' or to other factors. This review is divided into three parts. First, basic processing routes for nanocomposites, namely conventional powder processing, sol–gel processing and polymer pyrolysis are presented in detail. Second, the mechanical properties of different nanocomposites are compared. Finally, models which attempt to explain the improvements in these properties are explored. It will be shown that the strength increase can best be related to a reduction in processing defect size. For applications the most interesting properties of nanocomposites are their wear, creep and high temperature performance. © 1997 Elsevier Science Limited.

1 Introduction

Although nanocomposites can be found in nature in the form of biological systems, such as plants and bones, the term and the concept 'nanocomposite' were formally adopted for ceramic materials by Roy, Komarneni and colleagues about a decade ago.[1–3] They developed hybrid ceramic-metal nanocomposite materials synthesised by sol–gel processes and discussed quasi-crystalline one- or two-component materials, with isolated phases or regions of 1–10 nm with different structure and/or composition.[1]

Nanocomposite materials can be defined as composites of more than one Gibbsian solid phase where at least one of the phases shows dimensions in the nanometre range.[1] The solid phases can exist either in amorphous, semicrystalline or crystalline states. The concept of structural ceramic nanocomposites was proposed by Niihara in 1991 and can be seen as an adoption of the nanocomposite approach for the microstructural tailoring of structural ceramic composites.[4–5] This work was mainly based on results obtained on the Si_3N_4/SiC[6] and Al_2O_3/SiC systems.[7]

Although this review is restricted to structural ceramic nanocomposites, Table 1 provides a more general summary of several classes of synthetic nanocomposites together with some examples. Photosensitive glasses which show precipitation of silver halogenides might be the most common application of the nanocomposite approach.[8] However, of much wider applicability is the range of electroceramic nanocomposites for information and charge storage within the electronic industry. In the nanoscale, quantum effects can be utilised to modify energy states and electronic structures of components.[9] Conducting nanosized particles dispersed in a dielectric matrix (i.e. Ni in PZT) can improve dielectric properties.[10] Unique catalytic properties can be achieved with entrapment-type nanocomposites where, for example, fine metal clusters are supported in zeolites (three-dimensionally linked network structures with channels up to 1 nm).[11] The solution sol–gel technique, in particular, offers an opportunity to produce not only ultra-homogeneous materials but also heterogeneous or nanocomposite materials.[1–3] After crystallisation and densification those materials are appropriate for numerous applications, such as electronic or structural materials.

One of the major characteristics, and at the same time the greatest disadvantage, of ceramics is their brittleness. There are only a few concepts available to compensate for this disadvantage and to improve the strength. Following Griffith's approach, the fracture strength of brittle materials can only be improved by an increase in fracture toughness or by a reduction in critical flaw size.[20] Therefore, much effort has been invested in sophisticated processing technology to reduce the size and density of processing flaws.[21] However,

*Present address: GKSS Research Institute, Max-Planck-Strasse, D-21502 Geesthacht, Germany.

Table 1. Types of nanocomposite

Type of nanocomposite	*Examples*	*Refs*
Low temperature sol–gel derived nanocomposites	Mullite/SiO_2; Al_2O_3/SiO_2; SiO_2/MgO; Al_2O_3/TiO_2; AlN/BN; Fe_xN/BN; mullite/ZrO_2; mullite/TiO_2	1–3, 12–13
Structural ceramic nanocomposites	Al_2O_3/SiC; Si_3N_4/SiC; MgO/SiC; Mullite/SiC	4–7
Glass ceramics; glass/metal nanocomposites	Photosensitive glasses	8, 14
Electroceramic nanocomposites	Co/Cr;	9
Nanocomposites films nanocomposites	Lead zirconate titanate (PZT)/nickel	10
Entrapment-type	Zeolite/metallic or zeolite/organic complexes	11
Layered nanocomposites	Pillared clays (montmorillonite/oxide sol particles)	15
Metal/ceramic nanocomposites	Fe–Cr/Al_2O_3; Ni/Al_2O_3	16,17
Organoceramic nanocomposites	Polymeric matrix/$PbTiO_3$	18, 19

the design of tougher, flaw-tolerant ceramics is a more interesting approach for wider industrial applications since it improves the reliability of a component. The fracture toughness can be increased by incorporating various energy-dissipating components into the ceramic microstructure.[22–24] These components can be inclusions such as whiskers, platelets or particles. The reinforcements serve to deflect the crack or to provide bridging elements hindering further opening of the crack. Another concept is to incorporate metallic ligaments into the ceramic matrix[25] to form crack bridging elements that absorb energy by plastic deformation. Finally, much benefit has resulted from incorporating a second phase which undergoes a phase transition in conjunction with a volume expansion initiated by the stress field of a propagating crack; this, too, can apply a closing force on the crack.[26]

Currently, it is not clear which, if any, of the above toughening and strengthening mechanisms apply to ceramic nanocomposites. The aim of this review is to develop a rational path for the optimisation of structural nanocomposites on the basis of current observations and consequent hypotheses. Particular emphasis will be given to Al_2O_3 matrices containing nanosize SiC particles and to Si_3N_4 containing SiC because these systems have been the subject of the greatest study.

2 Al_2O_3/SiC Nanocomposites

2.1 Processing

Following the initial work of Niihara and his co-workers,[7] several research groups have tried his processing route. However, owing to the limited details provided and to the need to establish cost-effective processing routes, different methods such as conventional powder processing, sol–gel processing and polymer processing have been developed. These all seek a homogeneous dispersion of the SiC nano-reinforcement in an Al_2O_3 matrix.

2.1.1 Conventional powder route

Generally, conventional powder processing for nanocomposites can be divided into four main steps: (1) selection of the raw materials, (2) wet mixing of the powders, (3) drying the slurries and (4) consolidation.

2.1.1.1 Raw materials. Table 2 compares the details of the main processing steps from selected papers. The most important requirements for the raw powders are small average particle size and high purity. Only ultrafine powders for both the matrix and the nano-reinforcement can guarantee satisfactory dispersion of the nano-phase in the final product. High purity powders are necessary to avoid the formation of a second phase during sintering.

Both γ-Al_2O_3[27–31] and α-Al_2O_3[32–38] powders can be used as raw materials for the matrix. The main advantages in the use of γ-Al_2O_3 powder are its loosely packed morphology and high surface area. The difference between α- and β-SiC powders results in different surface chemistry, thus affecting their dispersion behaviour. Generally, for mixing in water-based slurries, α-SiC is preferable.[38] α-SiC is produced via an Acheson carbothermal reduction and a subsequent milling process whereas β-SiC is produced by gas phase reaction of silicon halogenides with hydrocarbons.

2.1.1.2 Powder mixing. The homogenisation of the powder mixtures can be achieved by either wet ball milling or attritor milling techniques in both organic[27–33] or aqueous media.[34–38] Investigations of several organic media revealed large differences in their ability to stabilise the powder slurries. It has been reported that methanol leads to a consid-

Table 2. Comparison of classical powder processing methods for Al_2O_3/5 vol% SiC nanocomposites

	Niihara et al. *(27–32)*	*Stearns* et al. *(33)*	*BRITE/EURAM II project (34–38, 58,59)*
(1) Selection of raw materials	γ-Al_2O_3 (Asahi Chemicals Co., Tokyo)	α-Al_2O_3 (AKP53, Sumitomo, Osaka)	α-Al_2O_3 (AKP53, Sumitomo, Osaka)
	β-SiC (Ibiden Co Ltd, Ogaki)	β-SiC (Performance Ceramics Co., Peninsala, OH)	α-SiC (UF45, Lonza, now H.C. Starck, Germany)
(2) Mixing	Ball-milling with Al_2O_3 balls in highly pure ethanol, acetone or toluene (24 h)	Ultrasonic bath Ball-milling with ZrO_2 balls in methanol (48 h)	Ultrasonic finger Attrition-milling in water
(3) Drying	Not specified	Under infrared lamp	Freeze drying
(4) Consolidation	Hot-pressing (1600°C, 30 MPa, N_2)	Pressureless sintering or hot-pressing (1700°C, N_2)	Hot-pressing (1550–1700°C, 25 MPa, Ar)

erable deflocculation and can therefore be recommended.[33,38] However, aqueous powder mixing gives the opportunity for cost-efficient and non-hazardous fabrication. The zeta-potentials of α-Al_2O_3 and α-SiC aqueous suspensions as a function of pH are shown in Fig. 1. The α-$Al_2$3 powder has its isoelectric point at pH = 9 and a minimum viscosity at the same pH level.[39] Therefore, pH levels for water-based slurries should be higher than 9. This is readily achieved by dispersing alumina powder in water, due to its basicity.

Properties of the slurries and, therefore, the homogeneity of sintered nanocomposites can be further improved by using modified powders. Prior to mixing, the surface of the SiC powder can be modified using functional silanes[39–41] or a short-chained polyacrylic acid.[39] For processing in water, the dispersion of the Al_2O_3/SiC powder slurries[34–36] can effectively be increased with an ammonium polycarboxylate dispersing agent.

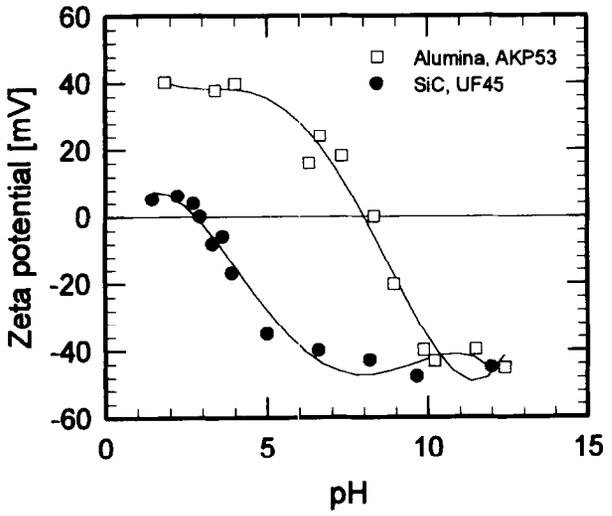

Fig. 1. Zeta-potential of alumina (AKP53, Sumitomo) and silicon carbide (UF45, Lonza) aqueous suspensions as function of pH (after Ref. 37).

To break up agglomerates in the SiC powder, ultrasonic dispersion and sedimentation techniques prior to mixing with the Al_2O_3 powder have been used successfully. Xu *et al.* reported that the average particle size was drastically decreased from 0·63 μm to 0·17 μm after a sedimentation treatment.[42]

Most critical is the drying of the slurries because of the risk of forming agglomerates. Surprisingly, in the publications of Niihara and his co-workers this detail is not mentioned. Stearns *et al.* used an infrared heat lamp to dry the slurry slowly in a bowl.[33] Fast drying rates at higher temperatures can result in hard agglomerates. We have found that freeze drying is the optimal procedure for the drying of aqueous suspensions. The short time necessary to freeze the whole slurry surpresses agglomerates and avoids segregation.[34–36] Usually, the dried powders or the green compacts have been calcined at 600°C for 10 h in air to remove organic dispersants.

2.1.1.3 Consolidation. Although expensive, hot-pressing has predominantly been used for the consolidation of nanocomposites. Generally, hot-pressing is carried out using a graphite die, with pressures between 20 and 40 MPa, and temperatures between 1550 and 1800°C, all under Ar or N_2 atmospheres. The temperature necessary for a fully dense alumina-based nanocomposite with 5 vol% SiC is 1600°C, with 10 vol% SiC 1700°C and with 17 vol% up to 32 vol% 1800°C, respectively.[27–32]

Slip casting,[39–40] injection moulding[43] and pressure filtration[44] have all been used to produce green compacts with densities of up to 62% for pressureless sintering. The final densities of nanocomposites fabricated by pressureless sintering are usually somewhat lower compared to

materials densified by hot-pressing and do not exceed 98·5% of the theoretical value.[33,39,40] There are a large number of critical processing parameters for pressureless sintering. Most important is the preparation of the green compact and the atmosphere during sintering which can be influenced by the type of furnace, the composition of a powder bed and the inert gas. Cold-isostatic pressing or slip casting, sintering temperatures between 1700 and 1800°C, an N_2 atmosphere and graphite heated furnaces lead to the highest densities.[33,40]

2.1.1.4 Microstructures. Figure 2 shows typical TEM micrographs comparing the microstructures of an Al_2O_3/SiC nanocomposite and of a monolithic alumina (details, see Ref. 36). To produce similar alumina grain sizes in both materials, the monolithic alumina was hot-pressed at 1550°C whereas the nanocomposite was hot-pressed at 1700°C. SiC particles are located both within the alumina matrix grains and at Al_2O_3/Al_2O_3 grain boundaries. Note that the grain boundaries in the nanocomposite are not as straight as they are in the monolithic alumina. These irregularly curved grain boundaries result from a pinning effect as discussed later.

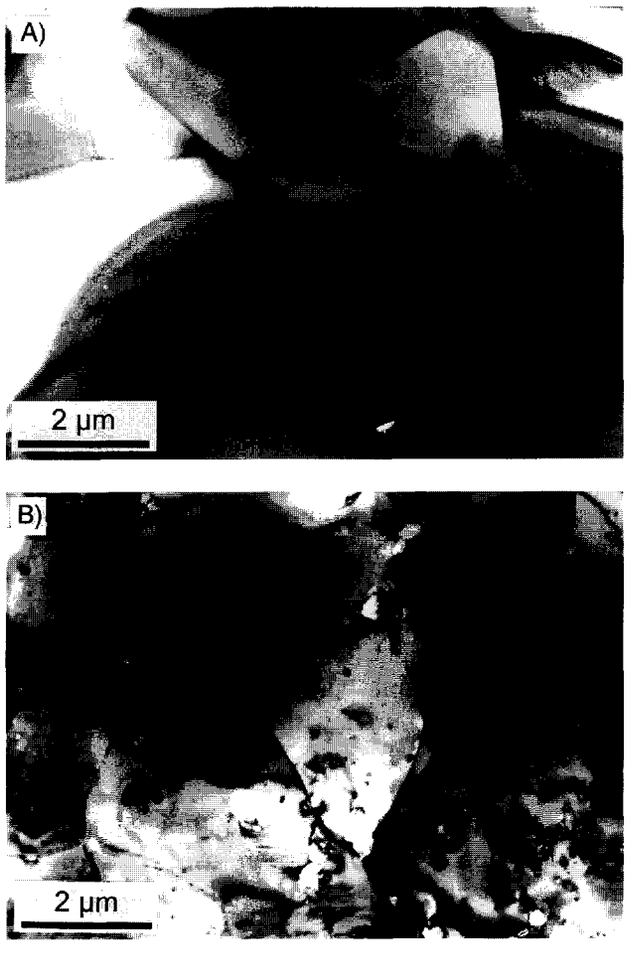

Fig. 2. TEM micrographs of (A) monolithic alumina and (B) an Al_2O_3/5 vol% SiC nanocomposite.

Another important feature of the nanocomposite microstructure is the occurrence of dislocations.[4,5,45] Dislocations are generated during cooling down from fabrication temperature due to high internal stresses near SiC particles. Furthermore, dislocation networks and subgrain or low angle grain boundaries are widely observed[4,5,45] and can be seen in Fig. 2. The importance of subgrain boundaries is that they can further refine the scale of the microstructure.

2.1.1.5 Post-annealing. Post-annealing has been used for a further increase of the strength of polished three-point or four-point bend test specimens.[27–33] To avoid oxidation the annealing was carried out under a reducing atmosphere at 1300°C for 1 h.

2.1.1.6 Thermodynamic stability at high temperatures. Impurities in the raw materials play an important role during the sintering because of the formation of a liquid phase. It is well known that during sintering of SiC containing metallic impurities in a nitrogen atmosphere, N_2 molecules can be activated by a dissociation chemisorption process on the surface of the SiC particles with the metallic impurities acting as catalyst.[46] Silica present at the surface of the SiC particles can then react to form Si_3N_4, according to:

$$3SiO_{2(l)} + 2N_{2(g)} \xrightarrow{Fe,C} Si_3N_{4(s)} + 3O_{2(g)}$$

In Al_2O_3/SiC mixtures Si_3N_4 can react with Al_2O_3 to form β'-sialon.

Apart from the impurity-catalysed reactions, decomposition reactions can occur in the Al_2O_3/SiC system during sintering. The thermal stability of an Al_2O_3/5 vol% SiC nanocomposite in air at 1400°C as a function of time has been studied by Wang *et al.*[47] At high temperatures, SiC particles in the surface layer oxidise to form silica which can react with alumina to form mullite. The time dependence of the formation of the reaction layer follows a linear rather than a parabolic function. This has been explained in terms of the formation of microstructural defects like pores after the oxidation of the SiC particles in the reaction layer. After 90 h at 1400°C in air, a reaction layer of 40 μm is found.

Studies of the thermodynamics of the Al_2O_3/SiC composite system[48,49] have shown that, even in an Ar atmosphere, Al_2O_3/SiC powder mixtures are not stable at temperatures above 1700°C. During sintering, high weight losses are observed due to volatilisation and decomposition of SiC leading to a high dissociation pressure. SiC vapour can react with Al_2O_3 to form a gaseous mixture of

SiO, Al_2O and CO.[48] Additionally, the formation of Al_4O_4C is observed. At temperatures above 1950°C a liquid can form through a reaction of SiC with Al_2O_3. If the SiC powder contains free carbon, the liquid phase will consist of Al. If not, Al_2O_3–Al_4C_3 or SiC–Al_4C_3 eutectic melts form. The reactions described are relevant for liquid phase sintering whereas, during hot-pressing, the consolidation is accelerated and takes place at much lower temperatures and the reactions themselves are suppressed. This may explain the difficulties experienced in pressureless sintering.

2.1.2 Polymer precursor route

The classical powder processing route possesses some limitations for the distribution of ultrafine (<50 nm) SiC powder due to agglomeration and dispersion problems. An alternative method of preparing Al_2O_3/SiC nanocomposites with ultrafine SiC particles is the pyrolysis of an Si-containing polymeric precursor.[50–52] The polymer (polycarbosilane) is coated onto a surface-modified alumina powder and pyrolysed at 1500°C to produce ultrafine SiC particles with a size of less than 20 nm.[51] The powder is hot-pressed at 1700°C, forming a fully dense nanocomposite.[51] The microstructure of this unique material is presented in Fig. 3; it consists of uniformly dispersed SiC particles which are much finer than those found in the conventional powder processed material shown in Fig. 2(b).

2.1.3 Sol–gel processing

Boehmite gels have been used as a source for Al_2O_3 that is either coated on crystalline nanosized SiC particles[42,53] or mixed with polysilastyrene, an SiC precursor, to produce Al_2O_3/SiC nanocomposites.[54] A 14 wt% boehmite powder and deagglomerated SiC is mixed with distilled water at pH = 3·5 for 6 h to form a transparent sol. After drying and calcination, the ultrafine powder is hot-pressed at 1600°C.[42] Compared to nanocomposites fabricated by conventional ball milling, sol–gel processing leads to smaller Al_2O_3 matrix grain sizes due to the better dispersion of SiC particles.

2.1.4 Final remarks on the processing of Al_2O_3/SiC nanocomposites

For the powder processing procedure, attritor milling in water, freeze drying and hot-pressing at 1550°C can be recommended. To establish cost-effective processing routes for industrial applications, however, more investigations on pressureless sintering at low temperatures have to be carried out. Such routes may be in conflict with the nanocomposite concept itself because grain growth and sinterability are drastically reduced by small inert particles.

Figure 4 compares conventional powder processing, polymer coating and the sol–gel route. The number of processing steps and the complexity for sol–gel and polymer processing are considerable but these methods may still prove to be attractive for industrial-scale production.

2.2 Mechanical properties

2.2.1 Density

Nanocomposites with considerably improved mechanical properties have, to date, only been achieved in hot-pressed materials. The strength depends on relative density and decreases with increasing porosity. This might explain why Zhao *et al.*[55] found almost no strength increase in pressureless sintered Al_2O_3/5 vol% SiC nanocomposites with a density of 98·3% whereas in hot-pressed

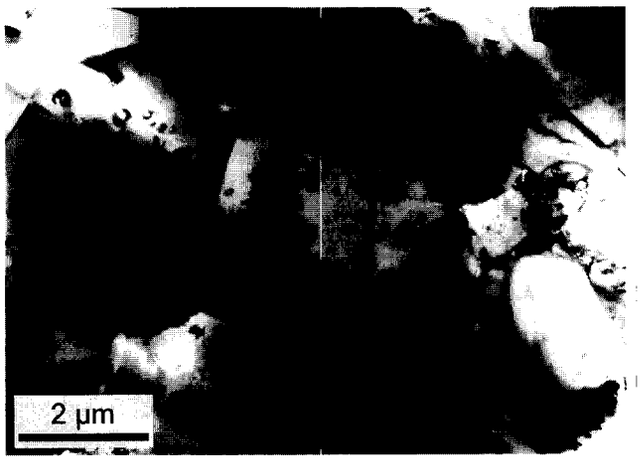

Fig. 3. TEM micrograph of an Al_2O_3/5 vol% SiC nanocomposite fabricated by the polymer coating route.

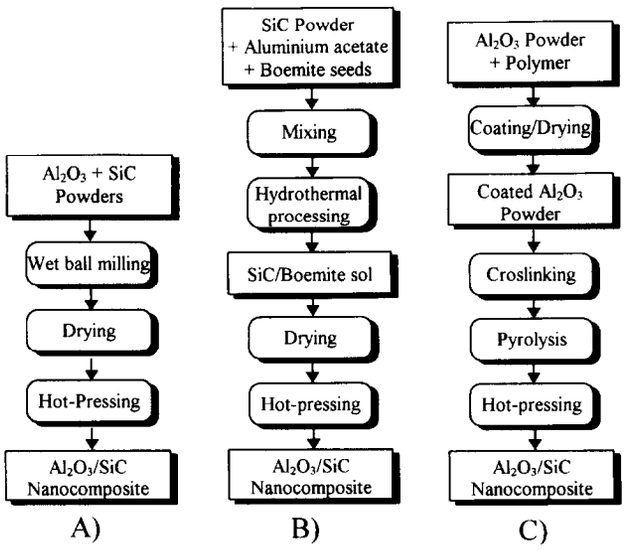

Fig. 4. Flow chart representing the processing of Al_2O_3/SiC nanocomposites by (A) classical powder processing, (B) sol–gel processing and (C) the polymer coating route.

materials with a density of 99·9% considerable increases in strength can be achieved. As mentioned in Section 2.1.1.6, possible decomposition reactions in the Al_2O_3/SiC system at temperatures above 1700°C and the formation of a second phase can play an important role for the density and, therefore, the strength of pressureless sintered nanocomposites.

2.2.2 Hardness and Young's modulus

Nakahira & Niihara[56] investigated the influence of hot-pressing temperature on density. They found that the hardness follows a linear rule of mixture as a function of SiC content up to 30 vol% SiC for Al_2O_3/SiC nanocomposites hot-pressed at 1800°C. For an Al_2O_3/5 vol% SiC nanocomposite the linear rule of mixture leads to a hardness of 17·5 GPa and a Young's modulus of 404 MPa compared to a hardness of 17 GPa and a Young's modulus of 400 MPa for alumina.

2.2.3 Fracture strength

Figure 5 shows a comparison of strength and fracture toughness of alumina-based nanocomposites at room temperature as a function of SiC content as presented in several papers. The strength of the monolithic alumina used as a reference varies from 350 to 560 MPa depending on the study. Therefore, a given relative improvement can be misleading. Following Niihara's original work,[4–7,27–32] the addition of only 5 vol% nanosized SiC increased the strength to 1050 MPa. A further increase of SiC content lowers the strength to a constant value of approximately 800 MPa. However, Niihara[27–32] explains the decrease of strength value for higher SiC contents by agglomeration problems.

A comparison of Niihara's results with those of other researchers, as shown in Fig. 5, leads to the conclusion that the strength of Al_2O_3/SiC nanocomposites reaches a plateau value of approximately 800 MPa for SiC contents of more than 10–20 vol%. Large discrepancies, however, exist for nanocomposites with 5 vol% SiC; the very high strength values reported by Niihara and his co-workers have not been reproduced by other groups. The reason for this discrepancy still remains unclear.

The matrix grain size in nanocomposites not only decreases with decreasing sintering temperature but also decreases with increasing SiC content. This has to be taken into account for a true comparison of mechanical properties of different nanocomposites. The strength of ceramics (σ) usually follows a Hall–Petch relation:

$$\sigma = \sigma_0 + Kd^{-1/2} \quad (1)$$

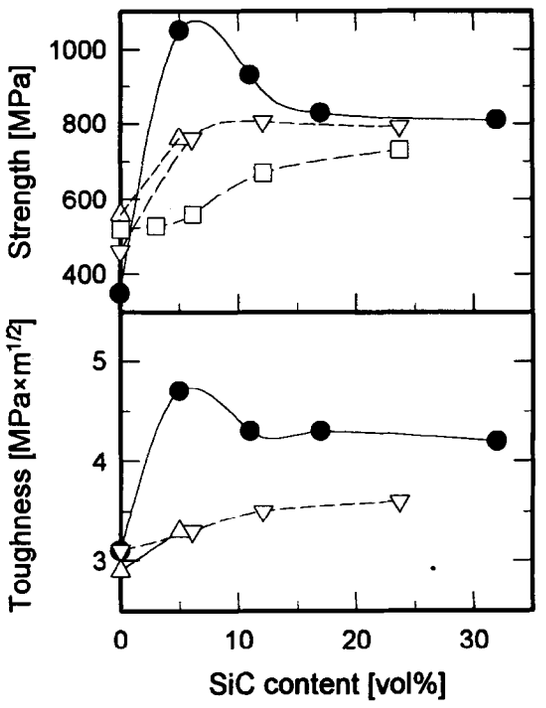

Fig. 5. Strength and toughness of Al_2O_3/SiC nanocomposites as a function of SiC content: (●) Niihara & Nakahira[29] by three-point bend test and Vickers indentation; (□) Borsa *et al.*[34] by four-point bend test; (△) Zhao *et al.*[55] by four-point bend test and indentation-strength method; (▽) Davidge *et al.*[58] by three-point bend test and notched beams.

This relation has been observed by Borsa *et al.*[34,35] for nanocomposites where the matrix grain sizes vary from 5·5 μm to 1·6 μm for SiC contents of 2·5 to 20 wt%. However, the nanocomposites investigated by Niihara *et al.*[27–32] are hot-pressed at different temperatures to produce the same average matrix grain size of 2 μm.

2.2.4 Annealing

Niihara reported that annealing polished specimens at 1300°C for 2 h in Ar increased the bend strength of an Al_2O_3/5 vol% SiC nanocomposite from 1050 MPa to 1540 MPa.[30] This phenomenon has also been observed by Zhao *et al.*[55] but they have found an increase from 760 to 1000 MPa. This improvement can possibly be related to the healing of machining-introduced cracks at the tensile surface of the bend test beams or to the relaxation of internal stresses (see Section 5).

2.2.5 Fracture toughness

The reported fracture toughness of nanocomposites is plotted in Fig. 5 as a function of SiC content. Niihara found a dramatic increase for 5 vol% SiC content and a decrease for higher SiC contents to 4·2 MPa$\sqrt{m}$.[29] Other researchers have reported modest increases in fracture toughness reaching a plateau value of approximately 3·5 MPa$\sqrt{m}$ for SiC contents of 10 vol% and more. The stress intensity factor K_I, measured as a function

of crack extension in an Al_2O_3/5 vol% SiC nanocomposite, showed a value of 2·1 MPa $\sqrt{m}$ with no R-curve behaviour.[57] The point in Fig. 5 with 5 vol% SiC found by Niihara and Nakahira[29] has not been reproduced by other researchers.

The fracture toughness of an Al_2O_3/5 vol% SiC nanocomposite has been measured by Zhao *et al.*[55] using an indentation pre-crack, followed by bend testing; this technique is less sensitive to machining-introduced stresses. It is found that the fracture toughness of nanocomposites is about 100% higher than the toughness for alumina when indentation crack length measurements are used. However, by using bend testing of pre-cracked beams an increase of only 20% is found. The authors conclude that the high toughness observed by Niihara *et al.*[27–32] is only apparent.

2.2.6 Fracture mode

One of the major differences between nanocomposites and monolithic alumina is the fracture mode which changes from mixed inter/transgranular to pure transgranular within the nanocomposites. This transition, which has been found by most researchers in the field, can clearly be seen in Fig. 6.

2.2.7 Wear behaviour

Probably the most important advantage of incorporating nanosized SiC particles in an alumina matrix is the increase in wear resistance, creep resistance and high temperature strength. The wear behaviour of nanocomposites has been investigated and compared to that of alumina as a function of matrix grain sizes.[58] Wear rates are measured by simple wet erosion experiments, using a slurry of alumina grit in water. The wear rate of the nanocomposites is reduced by a factor of about two over monolithic alumina with a similar grain size.[59] Two effects of the nanophase on wear have to be considered. First, the matrix grain size and, hence, the wear rate is reduced. Second, grain boundary fracture is inhibited during wear just as it is during fast fracture. Furthermore, a very fine-grained alumina (0·7 μm) for which wear occurs by plastic deformation yielding smooth surfaces has a higher wear rate than the nanocomposites. It appears that processes involving plastic deformation are also reduced.

2.2.8 Creep resistance

Thompson *et al.*[60] carried out tensile creep experiments on Al_2O_3/5 vol% SiC nanocomposites in the temperature range of 1200 to 1300°C under a constant load of 100 MPa. They found predominantly tertiary creep throughout the test whereas alumina, the reference sample, showed secondary creep. Microstructural investigations of the nanocomposites revealed cavities at the grain boundaries associated with SiC particles leading to failure. In Fig. 7, strain rates at 1% strain in a nanocomposite with 5 vol% SiC and in an alumina of 3·2 μm grain size obtained by Thompson *et al.*[60] are plotted together with results obtained by Nakahira *et al.*[61] for monolithic Al_2O_3 and an Al_2O_3/17 vol% SiC nanocomposite. Although the applied stresses and the SiC contents of the nanocomposites investigated are different, Fig. 7 emphasises the good creep behaviour of the nanocomposites.

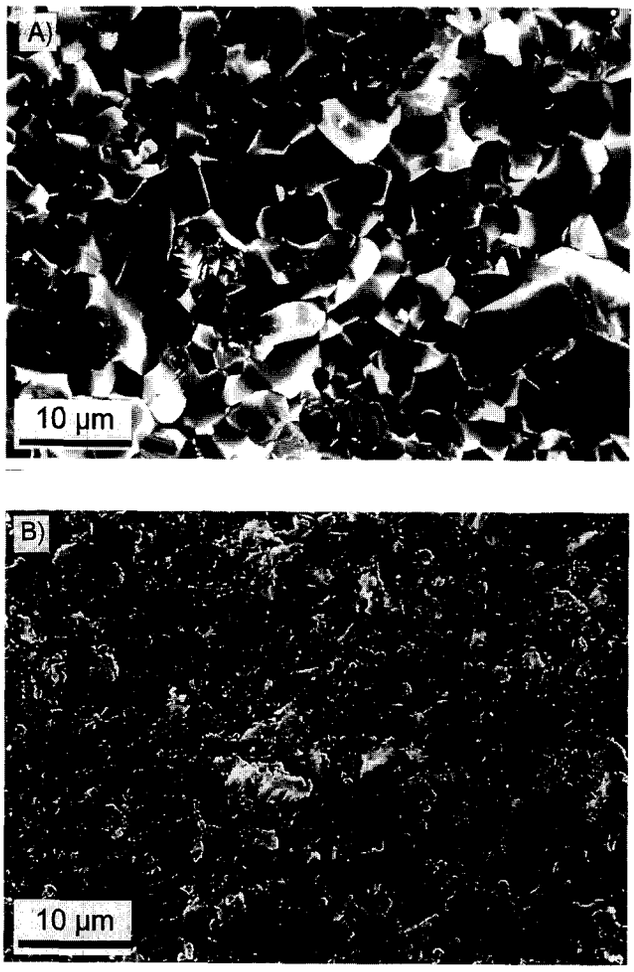

Fig. 6. Scanning electron micrographs of fracture surfaces of (A) monolithic alumina and (B) an Al_2O_3/5 vol% SiC nanocomposite obtained on four-point bend bars.

From TEM investigations, Ohji *et al.*[62] observed that the SiC particles at grain boundaries rotate while small cavities are formed. This underlines that the most important creep mechanisms, namely grain boundary sliding and dislocation movement, are drastically inhibited by nanosized SiC particles. The clamping and riveting mechanisms of SiC particles on grain boundaries become important.[63]

2.2.9 High-temperature strength

The strength of monolithic alumina starts to decrease above 800° and reaches values of about

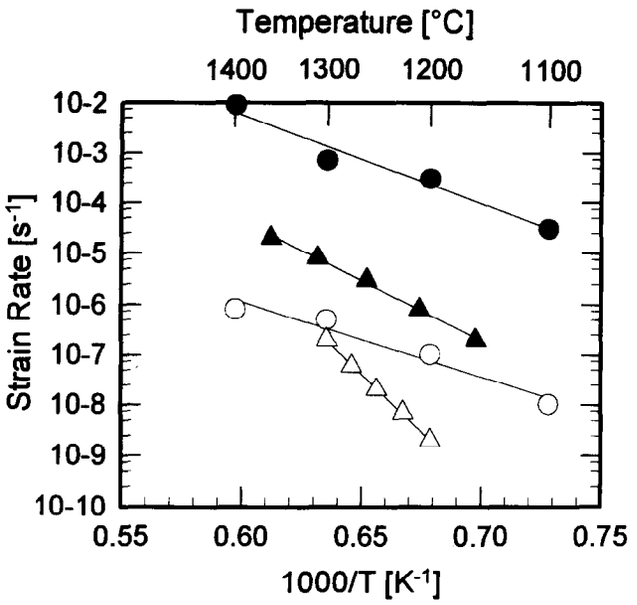

Fig. 7. Comparison of creep rates. Solid symbols represent monolithic alumina and open symbols represent nanocomposites; (○) Nakahira *et al.*[61]; (△) Thompson *et al.*[60]

30% of the room temperature strength at 1000°C. Depending on composition, Al_2O_3/SiC nanocomposites maintain their strength even up to 1000°C.[29,30] For higher temperatures, the strength drops drastically and reaches, for Al_2O_3/5 vol% SiC, nearly the same value as for alumina at 1400°C. The threshold temperature increases with increasing SiC content.

It has also been reported that the thermal shock resistance, measured by water quenching, is increased from 220°C for alumina to 420°C for an Al_2O_3/5 vol% SiC nanocomposite.[29]

3 Si_3N_4/SiC Nanocomposites

Si_3N_4 ceramics are attractive for high-temperature applications because they retain their high strength and good creep resistance. Already in the early 1970s, the reinforcement of Si_3N_4 ceramic matrix composites with micro-sized SiC particulates had been studied.[22] Greskovich and Palm[64] mentioned that the fracture toughness and microhardness of nano-sized SiC-reinforced Si_3N_4 appeared to be independent of the volume fraction of submicrometre-sized SiC up to 30 vol%. However, Niihara *et al.* have claimed that the strength and toughness of Si_3N_4/SiC nanocomposites are remarkably improved.[65–68]

3.1 Processing

3.1.1 Conventional powder processing

For conventional powder processing, commercially available α-Si_3N_4 powders (UBE grade E10) with an average particle size of 0·2 μm, produced by thermal decomposition of $Si(NH)_2$, have been mixed with up to 30 vol% β-SiC (Ibiden grade UF) and with 8 wt% Y_2O_3 as sintering aid. The powder mixtures were ball milled for 12 h in ethanol and hot-pressed at 1800°C in N_2 with 30 MPa.[65–68] Again, no details have been provided about the way the slurry is dried.

For the consolidation of Si_3N_4/SiC nanocomposites, various techniques were applied. Niihara *et al.* showed that for nanocomposites with more than 10 vol% SiC, a hot-pressing temperature of 1850°C was necessary to produce a fully dense material.[65–68] Akimune *et al.*[69,70] used cold isostatic-pressing at 400 MPa, pressureless sintering at 1700°C in N_2 for 3 h and then sinter-HIPing under 100 MPa for 1 h at 1850°C in a graphite crucible. Ishizaki and Yanai fabricated Si_3N_4/SiC nanocomposites[71] by reaction sintering of a modified Si_3N_4 powder. First, the surface oxygen content was adjusted by oxidation in air. Second, carbon was coated onto the Si_3N_4 powders by thermal decomposition of CH_4 gas at 800°C. High densities have been obtained by reaction sintering for high oxygen contents, especially at high carbon contents. Cold isostatic-pressing and gas-pressure sintering[72] as well as hot isostatic-pressing[73] have also been used.

3.1.2 Gas phase pyrolysis

The fabrication of Si_3N_4/SiC nanocomposite powders by vapour phase pyrolytic reaction is similar to the preparation of pure Si_3N_4 powders.[74] $[Si(CH_3)_3]_2NH$ or $[Si(CH_3)_2NH]_3$ are mixed with NH_3 in the ratio of 8 mol NH_3 to 1 mol Si together with Ar and then passed into a reaction chamber at 1000°C. The amorphous powder is collected and crystallised to Si_3N_4 in Ar at 1500°C for 6 h.[6] Si_3N_4/SiC nanocomposite powders are produced by using N_2 as a carrier gas and lower NH_3 contents. The carbon content in the as-received powder and thus the SiC content in the crystallised powder can be adjusted by the NH_3 content with a maximum value of approximately 34 vol% SiC in the final nanocomposite.[6] The resulting submicron powder is highly reactive and can react with oxygen or water to generate heat or even ignite. Therefore, an immediate heat treatment at 1350°C in Ar for 4 h is necessary. The further processing steps are as described above with 6 wt% Y_2O_3 and 2 wt% Al_2O_3[6,75–77] or, to improve the high-temperature properties of the Si_3N_4/SiC nanocomposite, with 8 wt% Y_2O_3 as sintering aids.[78,79]

3.1.3 Polymer pyrolysis

To produce Si_3N_4/SiC nanocomposites either an Si–C polymeric precursor can be coated onto fine

Si_3N_4 powder to produce SiC[80] or an Si–C–N polymeric precursor can be used to produce both Si_3N_4 and SiC.[81] For the powder coating route, mixtures of Si_3N_4 powder, sintering aids and the polymer, a polymethylphenylsilane, are attritor milled, cold isostatically-pressed, pyrolysed at 1000°C under Ar and, finally, pressureless sintered at 1850°C in N_2. The Si_3N_4/10 wt% SiC nanocomposite consists of micron-sized Si_3N_4 grains with well-dispersed SiC particles; it has a density of 96·7% TD.

Alternatively, polymethylsilazane can be converted through crosslinking and pyrolysis at 1000°C to an amorphous Si–C–N powder.[81-83] Again, the addition of sintering aids is necessary to promote liquid phase sintering. This requires attrition milling of the amorphous Si–C–N powder with 10·5 wt% Al_2O_3 and 4·5 wt% Y_2O_3. Pressureless sintering of the cold isostatic-pressed powder mixture at 1750°C leads to a composite of 97% TD and an SiC content of 24 wt%. The microstructure of the final composite is nano-crystalline for both the Si_3N_4 and the SiC phases with d_{50} = 0·2 μm; it shows a homogeneous SiC distribution.[81-83] Figure 8 compares both processing routes schematically. The microstructural development of the Si_3N_4/SiC composites derived by polymer pyrolysis depends strongly on the treatment temperatures of the polymer during preparation, crosslinking, pyrolysis and sintering.

The microstructure of an Si_3N_4/SiC composite fabricated by polymer processing[80] is shown in Fig. 9. Conventional powder processing leads to a micro/nano-microstructure with nanosized SiC particles dispersed mainly within the Si_3N_4 grains whereas polymer processing results in a nano/nano-type microstructure.

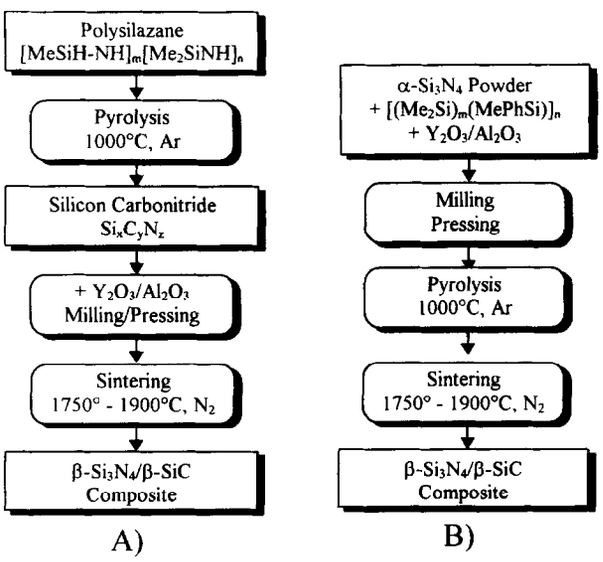

Fig. 8. Flow chart representing the processing of Si_3N_4/SiC (A) nano/nano and (B) micro/nano composites derived from organoelement precursors (after Refs 80–82).

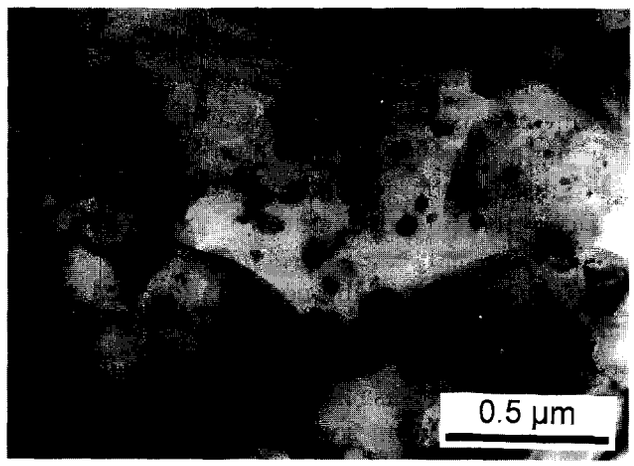

Fig. 9. TEM micrograph of Si_3N_4/10 vol% SiC composites fabricated by the polymer pyrolysis shown in Fig. 7B (courtesy R. Riedel & K. Strecker).

3.2 Mechanical properties of Si_3N_4/SiC nanocomposites

3.2.1 Strength and toughness

Figure 10 shows strength and fracture toughness for various Si_3N_4/SiC nanocomposites as a function of SiC volume fraction. All data were obtained from different publications of Niihara and his co-workers. Nanocomposites derived from the classical powder route are represented by solid symbols and nanocomposites fabricated from an amorphous Si–C–N powder by open symbols. With few exceptions, all data points follow a

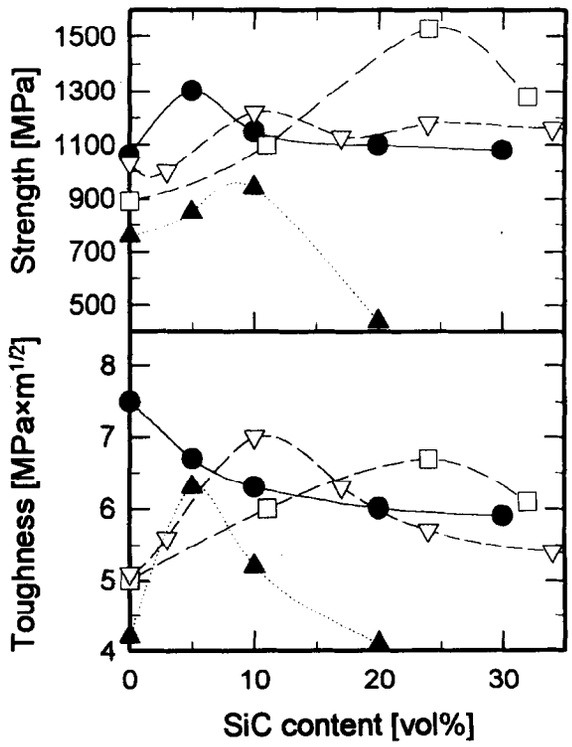

Fig. 10. Strength and toughness of Si_3N_4/SiC nanocomposites as a function of SiC content: (●) Ref 66; (△) Ref. 65; (□) Ref. 79; (▽) Ref. 84.

defined trend. The toughness increases from approximately 5 MPa$\sqrt{m}$ for monolithic Si_3N_4 to 6 MPa$\sqrt{m}$ for nanocomposites with ≥ 10 vol% SiC. This increase is accompanied by a modest increase in strength from 900 MPa to 1100 MPa.

To discuss the results in detail one has to consider the microstructure of the nanocomposites, especially the morphology of the Si_3N_4 grains. In the case of the powder processed materials, the decrease in fracture toughness and strength by addition of 20 vol% SiC has been related to a decrease in the relative density as well as to the formation of SiC agglomerates.[65] When using amorphous Si–C–N powders, no agglomeration problems occur even with high SiC contents.[79,84]

In Fig. 10 the high toughness in one of the Si_3N_4 reference samples with a value of 7·5 MPa$\sqrt{m}$ is associated with the presence of large elongated β-Si_3N_4 grains within the microstructure.[66] Generally, the addition of SiC leads to a refinement of the Si_3N_4 matrix grains and to a reduction in grain aspect ratio as can clearly be seen in Fig. 11 (SEM micrographs of fracture surfaces of monolithic Si_3N_4 and of an Si_3N_4/SiC nanocomposite). Furthermore, it is observed that the proportion of α-Si_3N_4 grains in Si_3N_4/SiC nanocomposites increases with increasing SiC content. The α–β phase transformation for Si_3N_4 is suppressed by the presence of SiC. The α–β transformation which occurs via a solution-precipitation process[85] appears to be hindered by nanosized SiC particles, especially if they are located at Si_3N_4/Si_3N_4 grain boundaries.

The mechanical properties of hot-pressed Si_3N_4 largely depend on composition, crystallinity and distribution of the sintering aids. The grain boundary phases consist of $Y_5N(SiO_4)_3$, Y_2SiO_5 and $Y_2Si_2O_7$ for monolithic Si_3N_4 as well as for the Si_3N_4/SiC nanocomposites fabricated with Y_2O_3 as sintering aid. Amorphous films were found at interfaces between intragranular SiC particles and the Si_3N_4 host grains as well as at interfaces at SiC particles located at Si_3N_4/Si_3N_4 grain boundaries.[86] Ishizaki and Yanai[71] suggested that the grain boundary phase itself is strengthened by SiC nanoparticles. These particles can also bridge two Si_3N_4 grains at their interface leading to an improvement in toughness and strength, especially when low SiC volume fractions are used. However, at higher SiC contents the effects of matrix grain refinement and homogenisation offset this improvement.

3.2.2 High-temperature properties

Si_3N_4/SiC nanocomposites show improved strength compared to Si_3N_4 up to high temperatures. An Si_3N_4/30 vol% SiC nanocomposite has a strength of almost 1080 MPa up to 1400°C whereas the strength of the monolithic reference sample is decreased considerably.[66] Furthermore, a reduced creep rate has been found for nanocomposites compared to monolithic Si_3N_4.[87] SiC particles act as bridging elements at the grain boundaries, thus hindering grain boundary sliding.

Several studies of the high-temperature properties of Si_3N_4/SiC nanocomposites have been published but a comparison is difficult because the softening behaviour of the sintering aids becomes important. Therefore, to rule out the influence of the glassy phase, Pezzotti and Sakai[88] have investigated a fully dense Si_3N_4/20 vol% SiC nanocomposite hot isostatically-pressed without sintering aids. No differences in strength and toughness were found between room temperature and 1400°C. The fracture toughness was measured by chevron-notched beam, by single-edge pre-cracked beam and by the indentation techniques.[88]

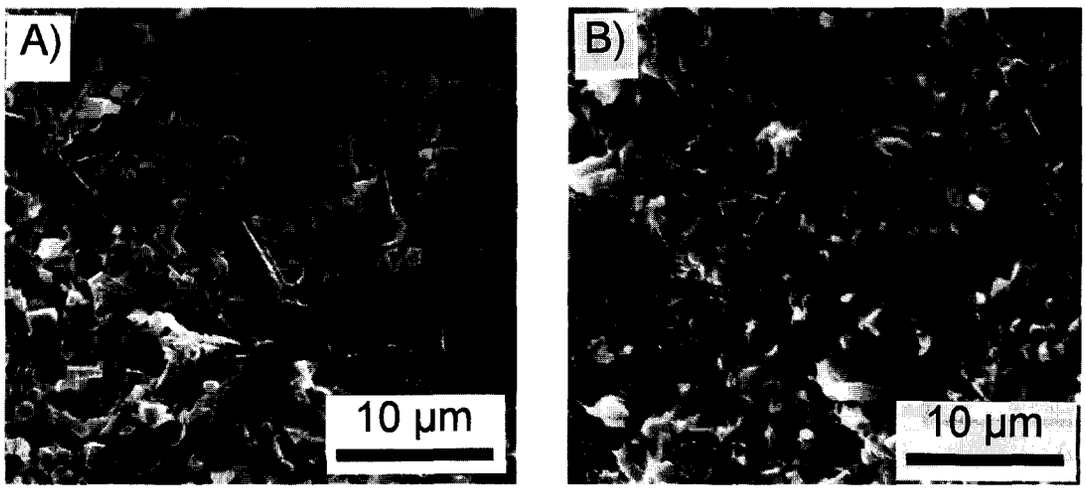

Fig. 11. SEM micrographs of fracture surfaces of (A) monolithic Si_3N_4 (8% Y_2O_3) and a Si_3N_4/20 vol% SiC (8% Y_2O_3) nanocomposite (courtesy A. Vaßen, Ref. 73).

Table 3. Other nanocomposite systems

System (matrix/particles)	*Processing method*	*Mechanical properties*	*Refs*
MgO/SiC	Ball-milling (ethanol) Hot-pressing (1800°C)	Improved strength and toughness	4, 5, 29, 30, 89
Al_2O_3/TiN	Attritor-milling (water) Hot-pressing (1700°C/25 MPa)	No strength increase	35
Mullite/SiC	Pressureless reaction sintering of kaolin, Al_2O_3 and SiC (1700°C)	Improved strength and toughness	90,91
Al_2O_3/ZrO_2	Ball-milling (ethanol) Hot-pressing (1650°C/25 MPa) or pressureless sintering + HIPing	Improved strength and toughness	92–94
Al_2O_3/Mo Al_2O_3/W	Ball-milling of fine Al_2O_3 and Mo/W powders (acetone) Hot-pressing (1400°C)	Improved strength and toughness	95,96
Carbon-fibre-reinforced Si–Al–O–N matrix composites/SiC	Starting materials: Al_2O_3, Si_3N_4, SiC powders, polysilazane and carbon fibres Filament winding and hot-pressing	Improved strength and toughness	97
Al_2O_3–SiC whisker composites/TiC	Wet-milling Hot-pressing (1859°C)	Improved strength	98
Al_2O_3–YAG composites/SiC	Ball-milling Hot-pressing	Not investigated	99
Al_2O_3/Cr_3C_2	Ball-milling (water) Hot-pressing (1400°C/25 MPa)	Not investigated	100
Al_2O_3/50 vol% TiC (Y_2O_3)	Attritor-milling Liquid-phase sintering (1750°C)	Not investigated	101
Al_2O_3/TiO_2	Sol–gel-processing	Not investigated	102
$MoSi_2/ZrO_2$	Ball-milling (1-butanol) Hot-pressing (1550°C)	Improved strength and toughness	103
B_4C/TiB_2	Ball-milling (ethanol) Hot-pressing (2150°C/30 MPa)	Improved strength and toughness	104
TiB_2/TiN	Polymer precursor route (polyborazylene/metal precursor)	Not investigated	105
SiAlON/SiC	Ball-milling of carbo-thermally produced SiAlON with Y_2O_3 and SiC Pressureless sintering (1780°C)	Improved strength and toughness	106

4 Other Nanocomposite Systems

The list of studied systems in Table 3 demonstrates that structural ceramic nanocomposites are not limited to Al_2O_3/SiC and Si_3N_4/SiC. Different phases such as SiC, TiN, TiC, TiO_2, ZrO_2, Cr_3C_2 or even refractory metals like Mo or W can be used as nano-reinforcements with Al_2O_3, Si_3N_4, mullite or SiAlON as the ceramic matrix. Because the great interest in nanocomposites the list of investigated systems is still expanding. Therefore, Table 3 cannot be complete but can indicate that even exotic systems like ceramic/metal- or fibre-composite/SiC systems are under consideration.

Concerning processing, conventional powder mixing routes combined with hot-pressing as described in Section 2 are typical for most nanocomposite systems; however, specific modifications have to be made. For example, reaction sintering can be used to fabricate mullite or SiAlON matrix materials. For details the reader may refer to the original papers.

Further attention needs to be paid to the MgO/SiC and Al_2O_3/TiN systems because they show specific properties which are important for the discussion in Section 5.

4.1 MgO/SiC

The fabrication of MgO/SiC nanocomposites is similar to that for Al_2O_3/SiC except in that it requires higher hot-pressing temperatures between 1700 and 1900°C depending on the SiC content.[4,5,29,30,89] Table 4 shows selected mechanical and microstructural properties for MgO/SiC nanocomposites. Again, room-temperature fracture strength is increased for the nanocomposites compared to monolithic MgO. Table 4 shows the Griffith flaw size (c) for different MgO/SiC

Table 4. Mechanical properties of MgO/SiC nanocomposites

Composition	*MgO grain size (μm)*	*Hot-pressing temperature (°C)*	*Strength MPa*	*Toughness MPa√m*	*Griffith flaw size (μm)*
MgO	15	n.n.	330	1·1	4·5
5 vol% SiC/MgO	3·0	1700	450	1·5	4·5
10 vol% SiC/MgO	2·3	1700	490	1·8	5·5
20 vol% SiC/MgO	n.n.	1800	560	2·8	10·1
30 vol% SiC/MgO	1·6	1900	530	3·3	15·7
50 vol% SiC/MgO	n.n.	n.n.	630	4·0	16·3

n.n. Not mentioned.

nanocomposites calculated from the given strength and toughness value using:

$$c = \left(\frac{K_{Ic}}{Y\sigma} \right)^2 \quad (2)$$

where Y is the stress intensity function of the crack (assumed = $2/\sqrt{\pi}$ in the case of a halfpenny crack). As shown in Table 4, the critical flaw size increases with increasing SiC content perhaps owing to the formation of SiC agglomerates. Following eqn (2), the strength increase for MgO/SiC nanocomposites can be fully explained by the observed improvement in toughness.

MgO containing more than 10 vol% SiC maintains its high fracture strength of about 550 MPa even at 1200°C. The creep resistance is also improved. Steady creep rates under a compressive load of 25 MPa at 1450°C are lowered by two orders of magnitude for 30vol% SiC/MgO compared to monolithic MgO.[89] Depending on stress and temperature, SiC particles have been thought to hinder diffusion mechanisms, movement of dislocations and grain boundary sliding.[89]

4.2 Al_2O_3/TiN

Walker *et al.*[35] have examined the effect of the addition of nanosized TiN to Al_2O_3. The ultrafine TiN (average particle size = 15 nm) and Al_2O_3 powders are attritor milled in water, freeze dried and, finally, hot pressed at 1700°C. Compared to SiC, nanosized TiN shows a smaller effect on grain boundary pinning. A modest matrix grain size reduction is accompanied by the occurrence of large (1 μm) TiN particles mainly located at the grain boundaries. The strength of Al_2O_3/TiN nanocomposites is not increased compared to alumina and the fracture mode is not changed.

5 Modelling (Strengthening and Toughening Mechanisms)

The evidence is that Al_2O_3/SiC nanocomposites show an explicit increase in strength accompanied by a modest increase in toughness. Furthermore, grain boundaries are strengthened in nanocomposites as manifested by the transcrystalline fracture mode as well as by the increased resistance to wear and creep. It is accordingly desirable to understand these improvements. This modelling section is divided into three parts, the first two following the Griffith equation (2) where strength can be improved by a reduction in critical flaw size (c-mechanism) or by an increase in fracture toughness (K-mechanism). The third part deals with grain boundary strengthening and with internal stresses.

5.1 Flaw size reduction (c-mechanisms)

5.1.1 Zener grain boundary pinning

One of the main features of nanocomposites is that matrix becomes refined on adding nanosized SiC.[4,5,33,34] Following the Hall–Petch relation (eqn (1)) a refinement of the grain size leads to higher strength. Furthermore, abnormal grain growth is reduced in nanocomposites, thus leading to a narrower grain size distribution. The effect of grain boundary pinning by small inclusions is described by Smith[107] after a semi-quantitative approach by Zener:

$$\bar{R} \cong \frac{3}{4} \frac{r}{V_f} \quad (3)$$

where $\bar{R}$ is the average matrix grain boundary radius of curvature, depending on the radius (r) and the volume fraction (V_f) of spherical inclusions. Equation (3) is often given in the form

$$\bar{D} \propto r/V_f$$

where $\bar{D}$ is the average matrix grain diameter.

In Fig. 12 the Zener model (eqn (3)) is compared with experimental data where $\bar{R}$ is plotted as a function of $1/V_f$. The radius of SiC nanoparticles used in the calculation was taken to be 150 nm, which is typical for the materials studied. The model agrees well with the experimental data but large deviations exist at large SiC volume fractions. However, one has to consider that SiC particles are not completely inert during sintering.

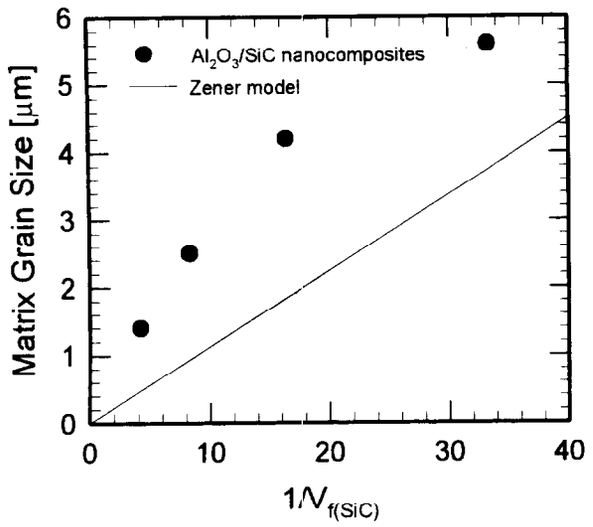

Fig. 12. Matrix grain size as a function of the inverse of the SiC volume fraction for Al_2O_3/SiC nanocomposites: (○) experimental data after Ref. 34; (—) prediction after eqn (3).

It has been found that α-SiC particles (UF45, Lonza) change their morphology from as-received irregular fragments to spherical after sintering.[36] Furthermore, for high SiC volume fractions SiC particles can form agglomerations or sinter together forming larger particles. This has to be taken into account if better agreement is to be obtained between the model and experimental results at high SiC volume fractions because eqn (3) predicts larger matrix grains for larger SiC particle sizes.

However, the reduction of the matrix grain size is obvious when taking into account that monolithic alumina sintered under the same conditions possess a much larger grain size of about 20 μm.

Equation (3) predicts that smaller SiC particles are even more effective for grain boundary pinning. However, studies of the SiC particle size effect in Al_2O_3-based nanocomposites confirm that the matrix grain size is independent of the SiC particle size for the same SiC volume fraction. Very small (20 nm) SiC particles are predominantly located within the matrix grains whereas larger SiC particles (300 nm) are located mainly at grain boundaries.

5.1.2 Dislocation networks

Another strengthening mechanism for Al_2O_3/SiC nanocomposites based on flaw size reduction has been presented by Niihara.[4,5] He proposes that strengthening arises due to the refinement of the microstructural scale from the order of the alumina grain size to the order of the interparticle spacing, thus reducing the critical flaw size. Indeed, the occurrence of subgrain or low angle grain boundaries is widely acknowledged. During cooling down, SiC particles can generate dislocations owing to internal stresses (see Section 5.3.1). At high temperatures these dislocations can propagate and form dislocation networks. However, Niihara's strength and toughness values for the Al_2O_3/SiC system of 1 GPa and 4·8 MPa$\sqrt{m}$, respectively, yielded a Griffith critical flaw size of 18 μm (see eqn (2)). A refinement of the microstructure from the average alumina matrix grain size of 1·5 μm to the average interparticle spacing of 200 nm plays, therefore, only a minor role.

Dislocation networks as shown in Fig. 13 have been investigated in detail by Jiao *et al.*[45] In Al_2O_3/SiC nanocomposites, perfect $\langle 1\bar{1}00\rangle$ dislocations and their dissociation can be observed. A shear stress of over 400 MPa on the $\{11\bar{2}0\}$ plane is necessary to activate the prismatic slip system with $\langle 1\bar{1}00\rangle$ dislocations. However, quantitative numbers for dislocation densities or low angle grain boundaries are not yet available.

5.1.3 Reduction in processing flaw size

A further explanation for the increased strength of the nanocomposites is a reduction in the size of processing flaws. Fractographical studies on broken four-point bend test beams have shown that the strength-determining processing flaws change in size and in morphology from large-volume pores in alumina to crack-like flaws due to SiC agglomerations in Al_2O_3/SiC nanocomposites.[36] The different processing flaw type results from the specific nanocomposite processing rather than from an intrinsic nanocomposite effect. In Al_2O_3/SiC nanocomposite powder mixtures, hard SiC agglomerates represent the predominant flaw type. It appears that the SiC particles act as a grinding medium during attritor or ball milling and successfully destroy soft Al_2O_3 agglomerates. The latter commonly cause large processing flaws such as voids in alumina ceramics. A typical processing flaw in a nanocomposite is shown in

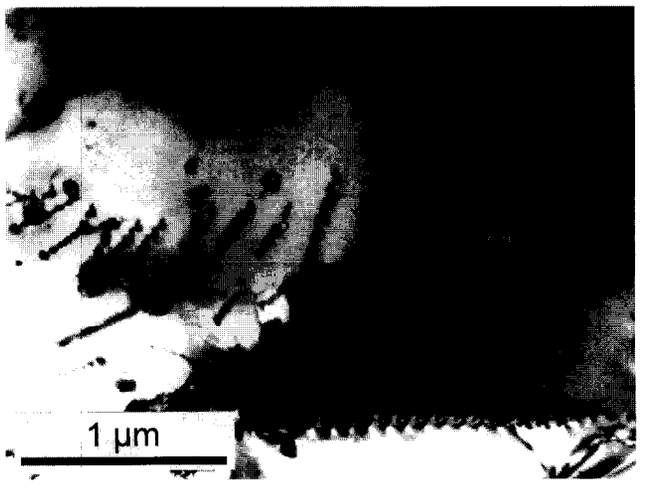

Fig. 13. TEM micrograph of an Al_2O_3/5 vol% SiC nanocomposite showing dislocation networks (courtesy S. Jiao).

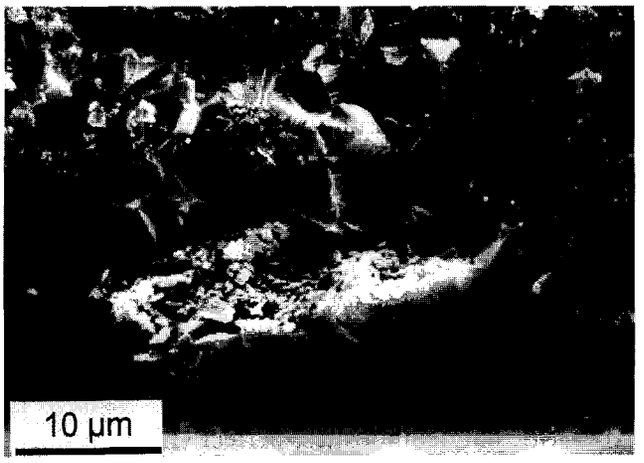

Fig. 14. SEM micrograph of a typical processing flaw in nanocomposites on a fracture surface near the tensile surface.

Fig. 14 in the form of an SEM micrograph of a fracture surface and in Fig. 15 by a schematic. The shape of the flaws in nanocomposites is similar to the crack-like voids produced by ZrO_2 agglomerates in Al_2O_3/ZrO_2 composites, as described by Lange *et al.*[108] The flaw morphology is similar to a volume pore which contains a large SiC polycrystal connected to the bulk nanocomposite by only half its surface (Fig. 15).

5.1.4 Crack healing (annealing treatment)

Zhao *et al.*[55] suggest that SiC particles only indirectly influence the strength by enabling the compressive stresses induced by the grinding process to be retained in the surface region of the test specimens. Another theory is that cracks in nanocomposites can heal during annealing. To explain the strength increase after annealing of polished four-point bend bars (see Section 2.2.4), the effects of crack healing and internal stress relaxation have been studied.[109,110] Alumina and Al_2O_3/SiC nanocomposites are indented with a Vickers pyramid to generate radial cracks. After annealing at 1300°C in Ar for 2 h the materials behave completely differently.[110] Whereas cracks in alumina grow, cracks in nanocomposites close, thus explaining the strength increase of annealed nanocomposites.

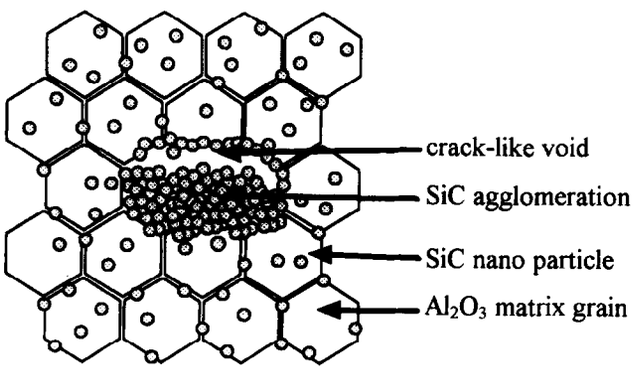

Fig. 15. Schematics of a typical processing flaw in nanocomposites.

Possible reasons for the crack healing have not yet been found and more systematic work is needed. However, by taking into account internal stresses, one has to distinguish carefully between the stresses introduced by the Vickers indentation (comparable to machining-introduced stresses), stresses introduced by the thermal expansion mismatch of Al_2O_3 and SiC and, finally, stresses due to the thermal anisotropy of alumina grains. Fang *et al.*[110] observed that residual stresses introduced by Vickers indentation fully relax in alumina after an annealing procedure whereas compressive stresses are still present in nanocomposites. Their observation is based on studying the crack lengths at satellite Vickers indentations around a primary indentation, before and after annealing. Again, more systematic work is needed.

5.2 Toughening (*K*-mechanisms)

5.2.1 R-curve effects

Concerning R-curve effects one has to distinguish between mechanisms acting on the crack wedge behind the crack tip and mechanisms acting directly at or in front of the crack tip. It is well known that monolithic alumina ceramics exhibits R-curve behaviour due to crack bridging mechanisms. The fracture mode is intercrystalline with partially connected grains acting as ligaments.[111] In nanocomposites any toughening effects acting on the crack wedge behind the crack tip are unlikely because of the lack of bridging elements. This is supported by the transgranular fracture mode. Therefore, only mechanisms acting directly at or in front of the crack tip can be assumed to be applicable to nanocomposites. Such microtoughening mechanisms do not necessarily lead to an increase in the toughness plateau value but they can result in a steep rise of the R-curve for very short crack lengths. This would explain a higher strength, as schematically shown in Fig. 16 where the crack resistance is plotted as a function of crack length. The slope of the tangents on the R-curves represents the strength.[111] By assuming the same initial flaw sizes and plateau toughness values, a higher strength can be achieved for a sharply rising R-curve. In the next chapters two mechanisms leading to sharply rising R-curves, namely crack deflection and crack bowing, are described.

5.2.2 Crack deflection

The interactions of a crack front with second-phase inclusions, such as spherical particles in nanocomposites, depend on the differences in the

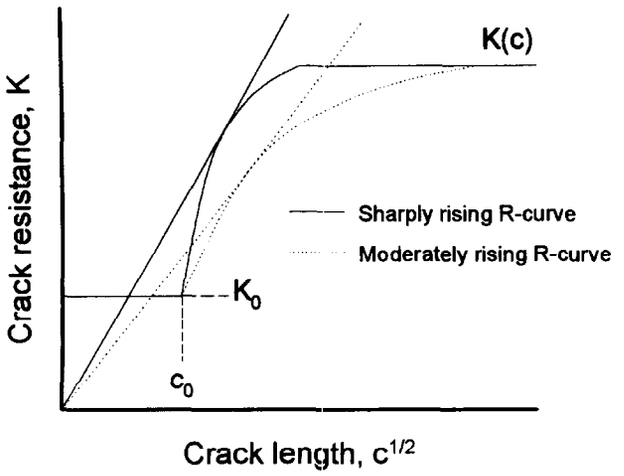

Fig. 16. Schematical dependence of the toughness as a function of crack length by assuming a steep and a flat rise for short crack lengths.

thermoelastic properties of the matrix and inclusions. If there are no differences, the planar crack front will not be influenced.[112] Following Faber and Evans,[113] in the case of such differences, the crack front will be deflected from planarity by a single particle or twisted between two neighbouring particles. The toughening of the composite is a result of diminishing the stress intensity directly at the tip of the deflected crack. The extent of toughening increase can be obtained by calculating the local stress intensities at the crack front. The toughness increase depends on the shape, volume fraction and interparticle spacing of the reinforcement. As discussed later, crack deflection can also explain the change in fracture mode.

Niihara has proposed a toughening effect due to crack deflection caused by compressive residual stresses around the SiC particles.[4,5] One requirement of the crack deflection theory is a strong interface between the SiC particles and the matrix. Investigations of SiC/Al_2O_3 interfaces, as presented in Fig. 17, revealed that the boundary is free of second phases.[114,28] An alignment of the SiC particles with the Al_2O_3 matrix can be observed in some cases.[114] These examinations suggest strong adhesion between the SiC particles and the matrix. Concerning SiC/Al_2O_3 interfaces at SiC particles located at Al_2O_3/Al_2O_3 grain boundaries, Jiao *et al.*[114] have estimated that the interfacial fracture energy between SiC and alumina is twice that of the alumina grain boundary fracture energy.

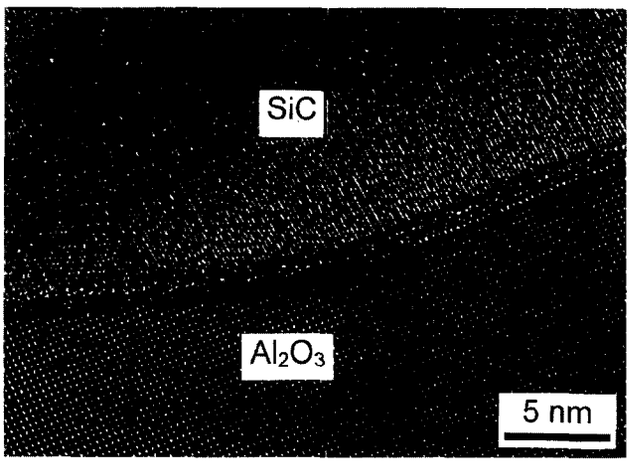

Fig. 17. TEM micrograph of an Al_2O_3/5 vol% SiC nanocomposite showing an Al_2O_3/SiC interface (courtesy S. Jiao).

Although there are evidences for crack deflection it is still difficult to give quantitative explanations. The evidences are that the fracture mode is changed in nanocomposites to transcrystalline fracture and crack deflection on SiC particles at Al_2O_3 grain boundaries were directly observed by TEM investigations.[115] However, TEM investigations are difficult to interpret because on a thin TEM specimen only two-dimensional information can be obtained. Therefore, a whole crack front cannot be observed.

5.2.3 Crack bowing

Particles in nanocomposites can also cause local changes in crack velocity. This effect can be described as crack bowing and has been proposed as a mechanism for increasing the fracture toughness of brittle materials. Green[116] has developed an analytical expression to characterise numerically the fracture toughness associated with the crack bowing effect. This expression depends on the free interparticle spacing, λ, but is independent of particle size. In nanocomposites a crack can rest at SiC particles but it is not clear if crack bowing occurs. Again, a whole crack front has to be investigated in order to study the effect of crack bowing.

Pezzotti *et al.*[117] have presented a theoretical approach for modelling toughness and strength in ceramic/ceramic and especially in ceramic/metal nanocomposites. Their model is based on the effect of the crack bowing effect. They conclude that, in contrast to metallic inclusions, ceramic nanosized dispersoids are completely ineffective on the material strength.

5.3 Grain boundary strengthening mechanisms

Several authors[35, 55, 59] have found that grain pull-out is significantly reduced in Al_2O_3/SiC nanocomposites during polishing, machining or abrasive wear. Furthermore, the fracture mode changes to transcrystalline. All these observations indicate that matrix grain boundaries are strengthened in nanocomposites. This effect is probably the most important difference between nanocomposites and the pure matrix. Conceivable reasons for the grain boundary strengthening are: (1) deflection of a

crack running along a grain boundary at an SiC particle into the grain (as discussed in Section 5·2), (2) strengthening of the grain boundaries due to local internal stresses. Therefore, internal stresses are discussed in detail in the following sections.

5.3.1 Thermal expansion mismatch (Selsing model)
Since the microstructures of nanocomposite ceramics are formed during sintering at high temperatures, differences in the thermal expansion coefficients of the matrix (α_{matrix}) and of the nano-particles ($\alpha_{particle}$) cause strains during cooling. These thermal expansion misfit strains, $\langle\alpha^*\rangle$, can be calculated by an integration over temperature. The upper limit is taken as the temperature below which plastic deformation is insignificant ($T_{plastic}$) and the lower limit is the room temperature.

$$\langle\alpha^*\rangle = \int_{T_0}^{T_{plastic}} (\alpha_{particle} - \alpha_{matrix})\, dT \qquad (4)$$

The thermal expansion misfit stress, σ_T, inside a single spherical inclusion in an infinite matrix can be described by the following expression after Selsing:[118]

$$\sigma_T = \frac{\langle\alpha^*\rangle}{\frac{1+\nu_m}{2E_m} + \frac{1-2\nu_p}{E_p}} \qquad (5)$$

E and ν are Young's modulus and Poisson's ratio of the matrix (m) and the particles (p). The tangential, σ_{Tt}, and the radial, σ_{Tr}, stress distributions in the matrix around the particle are given by:

$$\sigma_{Tt} = -\frac{\sigma_T}{2}\left(\frac{r}{x}\right)^3 \qquad \sigma_{Tr} = \sigma_T\left(\frac{r}{x}\right)^3 \qquad (6)$$

where r denotes the radius of the inclusion and x is the radial distance from the inclusion surface. Assuming $T_{plastic}$ as 1500°C and the room temperature thermoelastic data given in Table 5, eqn (5) leads to a compressive hydrostatic stress inside the SiC particles of 2·0 GPa for the Al_2O_3/SiC and 4·3 GPa for the MgO/SiC system. Tensile hydrostatic stresses of 500 MPa and 600 MPa can be calculated for the Si_3N_4/SiC and the Al_2O_3/TiN systems, respectively. Evidently, a change in fracture mode occurs only in systems with high compressive stresses within the nano-particles such as Al_2O_3/SiC and MgO/SiC.

Table 5. Thermoelastical data for matrix and nanophase

	E [*MPa*]	γ	$\alpha[10^{-6}\,K^{-1}]$
Al_2O_3	400	0·23	8·3
Si_3N_4	300	0·27	3·2
MgO	300	0·18	14
TiN	~470	~0·25	9·4
SiC	480	0·17	4·4

5.3.2 Average internal stresses
A model developed by Taya *et al.*[119] incorporates the influence of the particle volume fraction on the average residual microstress in the matrix for a composite material with spherical inclusions showing a thermal expansion mismatch. Their model is based on Eshelby's equivalent inclusions approach referring to the inelastic eigenstrains. The average residual microstresses inside the matrix and the particles, $\langle\sigma_m\rangle$ and $\langle\sigma_p\rangle$, are given by the following expressions:

$$\frac{\langle\sigma_p\rangle}{E_m} = \frac{-2(1-V_f)\beta\langle\alpha^*\rangle}{(1-V_f)(\beta+2)(1+\nu_m) + 3\beta V_f(1-\nu_m)}$$

$$\frac{\langle\sigma_m\rangle}{E_m} = \frac{2V_f\beta\langle\alpha^*\rangle}{(1-V_f)(\beta+2)(1+\nu_m) + 3\beta V_f(1-\nu_m)} \qquad (7)$$

$$\text{where } \beta = \frac{1+\nu_m}{1-2\nu_p}\cdot\frac{E_p}{E_m}$$

In the case of $\alpha_m > \alpha_p$, the average thermal stresses are compressive inside the particles and tensile in the matrix. For $V_f = 0$, eqn (7) provides the same value for the stresses inside the particles as the Selsing model.[118] Another boundary condition is given by mechanical equilibrium with $\langle\sigma_m\rangle(1-V_f) + \langle\sigma_p\rangle V_f = 0$.

Values of average residual stresses in the matrix and the inclusions for Al_2O_3/SiC nanocomposites have been measured by means of X-ray[120] and neutron diffraction[121] or by piezo-spectroscopy.[122] Although the techniques used are different (X-rays sample the surface of a specimen whereas neutrons sample the bulk material) the results are in good agreement. Figure 18 shows experimental results together with a prediction using eqn (7). A stress-free temperature of 1500°C, below which plastic deformation is insignificant, is assumed. (By considering that internal stresses at the

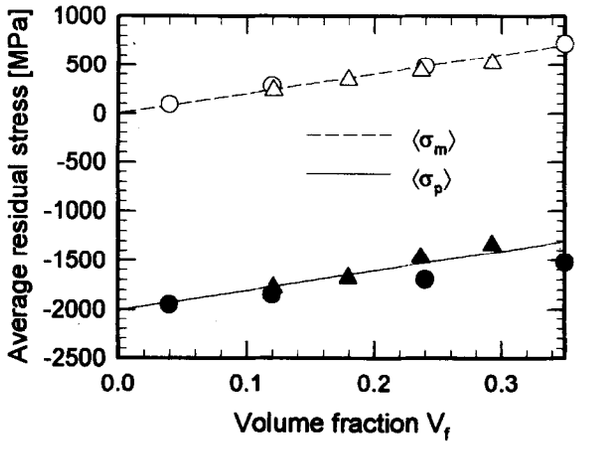

Fig. 18. Average residual microstresses in the matrix $<\sigma_m>$ and nano inclusions $<\sigma_p>$ for Al_2P_3/SiC nanocomposites. (△, ▲) Ref. 121; (○, ●) Ref. 120)

surface of a nanocomposite are not relieved after annealing at 1300°C, as observed by Fang *et al.*,[110] the stress-free temperature must be somewhere between 1300 and 1550°C which is the minimum hot-pressing temperature to get fully dense nanocomposites.) It has to be emphasised that all theoretical calculations concerning internal stresses depend strongly on values used for the thermoelastic properties of the matrix and inclusions.

Levin *et al.*[123] have presented a model for the influence of the SiC particles on the fracture toughness of nanocomposites. The average tensile stress field in the matrix due to the thermal expansion mismatch of Al_2O_3 and SiC reduces the fracture toughness. As shown in Fig. 18, the average microstress in the matrix is approximately 100 MPa for an Al_2O_3/5 vol% SiC nanocomposite. SiC submicron particles within the grains strengthen the grain boundaries because of compressive radial stress components, thus increasing the fracture toughness via a change in the fracture mode. It has been claimed that a net increase in toughness can only be achieved for small SiC volume fractions because the strengthening effect of grain boundaries is high and only in this case are the average internal stresses small. The maximum increase of fracture toughness at 5 vol% SiC as shown by Niihara[4] agrees with the model proposed by Levin *et al.*[123] and is plausible when taking into account the two opposite effects of grain boundary strengthening and average tensile internal stresses. However, this maximum in toughness for nanocomposites has not been reproduced by other workers.

The model proposed by Levin *et al.*[123] predicts that a further improvement in the toughness is possible by decreasing the SiC particle size because the average interparticle spacing is reduced whereas the average internal stresses remain unaffected. However, in a study of SiC particle size effects,[36,52] it has been observed that the fracture toughness decreases with decreasing SiC particle size, especially for ultrafine SiC particle distributions produced by polymer pyrolysis.

5.3.3 Local stress distribution

For discussion of the grain boundary strengthening effect due to internal stresses it is helpful to review the stress fields around the SiC particles. For the model presented in this review, a superposition of stresses in an arrangement of several particles including a grain boundary is assumed. Figure 19 shows the configuration assuming nine particles in a cubic-body-centred arrangement with an average nearest particle spacing equivalent to a SiC volume fraction of 2·5%. One particle is located in the plane. The remaining particles are

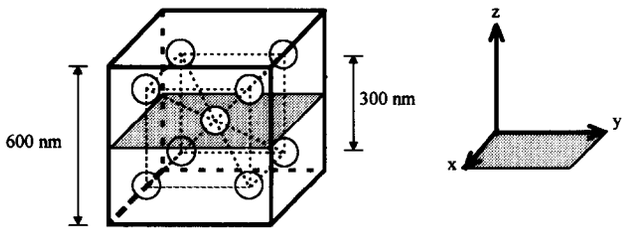

Fig. 19. Configuration for the stress distribution model in Fig. 20.

the same distance from that plane. Each particle causes a stress field which can be calculated using the Selsing equation (eqns (3) and (4)). The total stress at each point in the x-y-plane highlighted in Fig. 19 can easily be calculated assuming a simple superposition. For simplicity, only the superimposed stresses normal to the plane are plotted in Fig. 20. Obviously, the particle at the grain boundary generates high tensile stresses immediately around it and the other eight particles nearby to the plane generate compressive stresses up to 120 MPa. Figure 20 makes evident that SiC particles within the Al_2O_3 grains located close to grain boundaries strengthen the grain boundaries due to radial compressive stresses. The influence of SiC particles within grain boundaries is still unclear, but could be expected to generate countervailing tensions across the boundary.

5.4 Final remarks on strengthening and toughening mechanisms

Table 6 summarises all mechanisms discussed in the modelling chapter. The strength increase observed in nanocomposites can be explained by a decrease in critical flaw size. As shown above, not only is the size of processing flaws decreased but also their morphology changes completely. Furthermore, the matrix grain size is reduced with a

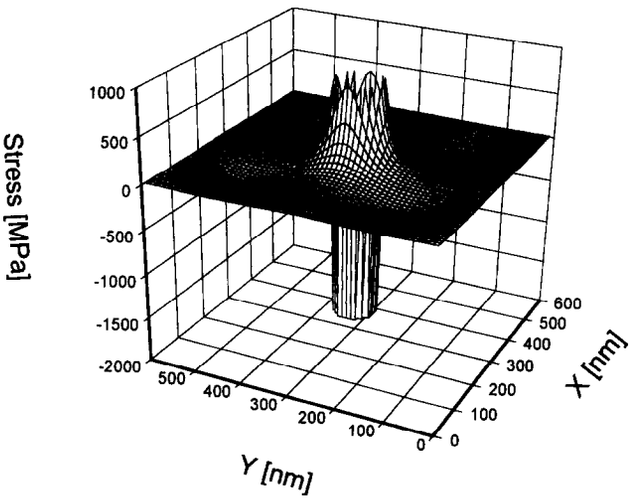

Fig. 20. Stress distribution normal to a plane caused by nine particles in a cubic body centered arrangement (see Fig. 19). ((+) tensile and (–) compressive stress).

Table 6. Summary of strengthening and toughening mechanisms

Mechanism	*Comment*	*Refs*
Zener grain boundary pinning (c-mechanism)	Matrix grain sizes are drastically reduced (typical for nanocomposites)	4, 5, 34
Dislocation networks (c-mechanism)	Refinement of microstructure is observed (no effect for strength increase)	4, 5, 45
Reduction in processing flaw size (c-mechanism)	Strength increase can be fully explained by observed change in processing flaw type (careful processing is very important)	36
Crack healing (c-mechanism)	Can explain strength increase after annealing (mechanisms are still unclear)	55, 109
R-curve effects (K-mechanism)	steep rising R-curve behaviour is proposed (no experimental evidence)	58
Crack deflection (K-mechanism)	Cracks seem to be reflected at SiC particles (importance for toughening is unclear)	113
Crack bowing (K-mechanism)	Experimentally difficult to verify (importance for toughening is unclear)	116, 117
Thermal expansion mismatch (grain boundary strengthening)	Fracture mode is changed to transcrystalline if $\alpha_{particle} < \alpha_{matrix}$ (e.g. for Al_2O_3/SiC)	4, 5, 55, 116–121
Average internal stresses (grain boundary strengthening)	Average tensile stresses in matrix if $\alpha_{particle} < \alpha_{matrix}$ (toughness is reduced)	119–123
Local stress distribution (grain boundary strengthening)	Local compressive stresses can strengthen grain boundaries if $\alpha_{particle} < \alpha_{matrix}$ (can explain change in fracture mode)	123, this paper

narrow size distribution due to the grain boundary pinning by inert SiC particles. Dislocation networks play only a minor role.

A clear identification of the toughening mechanism in nanocomposites remains difficult because, first, the toughness increase is small or even absent and, second, there is no single persuasive mechanism (Table 6). A balance exists between mechanisms decreasing toughness, i.e. average tensile internal stresses in the matrix, and mechanisms improving the toughness, i.e. crack deflection or grain boundary strengthening. All these mechanisms depend highly on specific processing and microstructural details. However, it appears that grain boundary strengthening due to local radial compressive stress components around SiC particles or due to a riveting effect is the most likely nanocomposite effect. The mechanism explains the transition in fracture mode as well as the improved resistance to wear and machining damage.

6 Outlook and Conclusions

Although interest in nanocomposites has increased over the last few years, it remains unclear to what extent the concept of structural ceramic nanocomposites represents a new approach to ceramic strengthening and toughening. This review has revealed that at least for the Al_2O_3/SiC system where the difference in thermal expansion between the matrix and the nano-inclusions leads to internal stresses, one can detect a clear nanocomposite effect. The change of the fracture behaviour to a transcrystalline mode, the reduced wear rates and the improved resistance against surface damage can be related to a grain boundary strengthening mechanism due to the nano-inclusions. However, several indirect effects relate to the SiC nano-phase. It seems that Al_2O_3 agglomerates, which usually lead to pore-like voids, are destroyed during nanocomposite powder processing. The only remaining flaws in the nanocomposites, i.e. SiC agglomerates, are smaller, thus increasing the strength. Another indirect effect is the reduction in matrix grain size compared to monolithic alumina due to the grain boundary pinning by inert SiC particles.

Since the incorporation of an inert nano-phase leads to a strengthening of the grain boundaries, nanocomposites have to be treated as one of the same family of toughening and strengthening approaches as whisker, metal ligament and zirconia reinforcement. Furthermore, the nanocomposite concept can be applied to a wide range of systems as shown in this review.

In the case of Si_3N_4/SiC nanocomposites, the assessment of a nanocomposite effect is even more complex. The difference in thermal expansion

coefficients of Si_3N_4 and SiC is much smaller than in the Al_2O_3/SiC system and has an opposite sign. A change in fracture mode is not observed and studies of surface damage as well as of wear resistance are yet not available. However, the most obvious effect is the strengthening of the glassy grain boundary phase explaining the improved high-temperature properties of Si_3N_4/SiC(Y_2O_3) nanocomposites.

As far as processing is concerned, methods that avoid or minimise handling of ultrafine powders, especially SiC powders, seem to be the most elegant. For both Si_3N_4- and Al_2O_3-based nanocomposites, the SiC nano-phase can be introduced *in situ* by the pyrolysis of a Si-containing polymeric precursor. For the Si_3N_4 system, reaction sintering with partially oxidised and carbon-coated Si_3N_4 powder is another example of *in situ* SiC formation.

The most interesting system for industrial application appears to be Al_2O_3/SiC. It has been demonstrated that conventional powder processing in an aqueous medium, slip casting and pressureless sintering represent a promising processing route for nanocomposites. However, improved strengths have not been reported for pressureless sintered nanocomposites. The reason may be the higher porosity.

Concerning the wear properties of Al_2O_3/SiC nanocomposites, several applications may be possible. For abrasive grits, fused alumina fulfils the requirements for a low-cost mass production material whereas super-abrasives, such as boron nitride or diamond, represent expensive materials and are of interest only for special applications. Al_2O_3/SiC nanocomposites, however, can fill the gap between these extremes with reasonable performance and an acceptable price.

Acknowledgements

The author would like to thank Prof. R. J. Brook, Prof R. W. Davidge and Dr B. Derby for their fruitful discussions. This project was supported by the EU (BRITE/EURAM II, Human Capital and Mobility contract No. ERB BRE2 CT94 3093).

References

1. Roy, R., Roy, R. A. and Roy, D. M., Alternative perspectives on 'quasi-crystallinity': Non-uniformity and nanocomposites. *Mater. Lett.*, 1986, **4**, 323–328.
2. Roy, R., Purposive design of nanocomposites: Entire class of new materials. In *Ceramic Microstructures 86, Role of Interface*, Vol. 21, 1987, pp. 25–32.
3. Komarneni, S., Nanocomposites. *J. Mater. Chem.*, 1992, **2**, 1219–1230.
4. Niihara, K., New design concept of structural ceramics—ceramic nanocomposites. *J. Ceram. Soc. Jpn.*, 1991, **99**, 974–982.
5. Niihara, K. and Nakahira, A., Structural ceramic nanocomposites by sintering method: Roles of nano-size particles. In *Ceramics: Towards the 21st Century*. The Ceram. Soc. of Japan, 1991, pp. 404–417.
6. Izaki, K., Hakkei, K., Ando, K., Kawakami, T. and Niihara, K., Fabrication and mechanical properties of Si_3N_4–SiC composites from fine, amorphous Si–C–N powder precursors. In *Ultrastructure Processing of Advanced Ceramics*, ed. J. M. MacKenzie & D. R. Ulrich. John Wiley & Sons, New York, 1988, pp. 891–900.
7. Niihara, K. and Nakahira, A., Strengthening of oxide ceramics by SiC and Si_3N_4 dispersion. In *Proc. 3rd. Int. Symp. on Ceramic Materials and Components for Engines*, ed. V. J. Tennery. Westerville Ohio, 1988, pp. 919–926.
8. Armistead, W. H. and Stookey, S. D., Photochromatic silicate glasses sensitized by silver halides. *Science*, 1964, **144**, 150–154.
9. Newnham, R. E., Size effects and nonlinear phenomena in ferroic ceramics. In *Third Euro-Ceramics*, vol. 2, ed. P. Durán and J. F. Fernández. Faenza Editrice Ibérica, Spain, 1993, pp. 1–9.
10. Kundu, T. K. and Chakravorty, D., Nanocomposite films of lead zirconate titanate and metallic nickel by sol–gel route. *Appl. Phys. Lett.* 1995, **66**, 3576–3578.
11. Özkar, S., Ozin, G. A. and Prokopowicz, R. A., Photooxidation of hexacarbonylmolybdenum(0) in sodium zeolite Y to yield redox-interconvertible molybdenum(VI) oxide and molybdenum(IV) oxide monomers. *Chem. Mater.*, 1992, **4**, 1380–1388.
12. Gonsalves, K. E., Xiao, T. D. and Chow, G.-M., Synthesis of nanocomposite materials via inorganic polymer gels. *ACS Symposium Series*, 1994, **572**, 195–206.
13. Colomban, P. and Mazerolles, L., Nanocomposites in mullite–ZrO_2 and mullite–TiO_2 systems synthesised through alkoxide hydrolysis gel routes: microstructure and fractography. *J. Mater. Sci.*, 1991, **26**, 3503–3510.
14. Chakravorty, D., Nanocomposites. *Bull. Mater. Sci.*, 1992, **15**, 411–420.
15. Yamanaka, S., Design and synthesis of functional layered nanocomposites. *Ceram. Bull.*, 1991, **70**, 1056–1058.
16. Laurent, C., Demai, J. J., Rousset, A., Kannan, K. R. and Rao, C. N. R., Fe–Cr/Al_2O_3 metal-ceramic composites: Nature and size of the metal particles formed during hydrogen reduction. *J. Mater. Res.*, 1994, **9**, 229–235.
17. Breval, E., Dodds, G. and Pantano, C. G., Properties and microstructure of Ni-alumina composite materials prepared by the sol/gel method. *Mater. Res. Bull.*, 1985, **20**, 1191–1205.
18. Krug, H. and Schmidt, H., Organic-inorganic nanocomposites for micro-optical applications. *New J. Chem.*, 1994, **18**, 1125–1134.
19. Messersmith, P. B. and Stupp, S. I., High-temperature chemical and microstructural transformations of a nanocomposite organoceramic. *Chem. Mater.*, 1995, **7**, 454–460.
20. Davidge, R. W., Mechanical behaviour of ceramics. Cambridge University Press, Cambridge, 1979.
21. Lange, F. F., Powder processing science and technology for increased reliability. *J Am. Ceram. Soc.*, 1989, **72**, 3–15.
22. Lange, F. F., Effect of microstructure on strength of Si_3N_4–SiC composite system. *J. Am. Ceram. Soc.*, 1973, **56**, 445–450.
23. Becher, P. F., Microstructural design of toughened ceramics. *J. Am. Ceram. Soc.*, 1991, **72**, 255–269.
24. Harmer, M., Chan, H. M. and Miller, G. A., Unique opportunities for microstructural engineering with duplex and laminar ceramic composites. *J. Am. Ceram. Soc.*, 1992, **75**, 1715–1728.
25. Sigl, L. S., Mataga, P. A., Dalgleish, B. J., McMeeking, R. M. and Evans, A. G., On the toughness of brittle materials reinforced with a ductile phase. *Acta Metall.*, 1983, **36**, 945–953.

26. Green, D. J., Critical microstructures for microcracking in Al_2O_3–ZrO_2 composites. *J. Am. Ceram. Soc.*, 1982, **65**, 610–614.
27. Niihara, K., Nakahira, A., Sasaki, G. and Hirabayashi, M., Development of strong Al_2O_3/SiC composites. *MRS Int. Mtg on Adv. Mater*, Vol. **4**, 1989, 129–134.
28. Niihara, K., Nakahira, A. and Inoue, M., Sintering process and mechanical properties for oxide-based nanocomposites. *Mater. Res. Soc. Symp. Proc.*, 1992, **271**, 589–593.
29. Niihara, K. and Nakahira, A., Strengthening and toughening mechanisms in nanocomposite ceramics. *Ann. Chim. Fr.*, 1991, **16**, 479–486.
30. Niihara, K. and Nakahira, A., Particulate strengthened oxide ceramic-nanocomposites. In *Advanced Structural Inorganic Composites*, ed. P. Vincenzini. Elsevier Applied Science, 1991, pp. 637–644.
31. Niihara, K. and Nakahira, A., SiC–Al_2O_3 composite sintered bodies and method of producing the same. European Patent, EP 0 311 289 B1, 27 Jan. 1993.
32. Nakahira, A. and Niihara, K., Sintering behaviors and consolidation process for Al_2O_3/SiC nanocomposites. *J. Ceram. Soc. Jpn*, 1992, **100**, 448–453.
33. Stearns, L. C., Zhao, J. and Harmer, M. P., Processing and microstructure development in Al_2O_3–SiC 'nanocomposites'. *J. Eur. Ceram. Soc.*, 1992, **10**, 473–477.
34. Borsa, C. E., Jiao, S., Todd, R. I. and Brook, R. J., Processing and properties of Al_2O_3/SiC nanocomposites. *J. Microscopy*, 1994, **177**, 305–312.
35. Walker, C. N., Borsa, C. E., Todd, R. I., Davidge, R. W. and Brook, R. J., Fabrication, characterisation and properties of alumina matrix nanocomposites. *Br. Ceram. Proc.*, 1994, **53**, 249–264.
36. Carroll, L., Sternitzke, M. and Derby, B., Silicon carbide particle size effects in alumina based nanocomposites. *Acta Metall. Mater.*, 1996, **44**, 4543–4552.
37. Poorteman, M., Deacamps, P., Cambier, F., O'Sullivan, D., Thierry, B. and Leriche, A., Optimisation of dispersion of nanosize SiC particles into alumina matrix and mechanical properties of corresponding nanocomposite. In *Proceedings of 8th CIMTEC*, Firence, 1994, in press.
38. O'Sullivan, D., Poorteman, M., Descamps, P., Cambier, F., Leriche, A. and Thierry, B., Optimisation of alumina –silicon carbide dispersions and the fabrication of nanocomposite ceramic materials. In *Key Engineering Materials*, Vol. **99–100**. Trans Tech Publications, Switzerland, 1995, pp. 247–255.
39. Assmann, S., Eisele, U. and Böder, H., Processing of Al_2O_3/SiC-composites in aqueous media. *J. Eur. Ceram. Soc.*, 1995, in press.
40. Aslan, M., Dörr, C., Nass, R. and Schmidt, H. Microstructural development and mechanical properties of pressureless sintered Al_2O_3/SiC composites. In *Ceramic Transactions*, **Vol. 51**, *Ceramic Processing and Science*, ed. H. Hausner, G. L. Messing and S.-I. Hirano. The American Ceramic Society, Westerville OH, 1995, pp. 665–669.
41. Jang, H. M., Rhine, W. E. and Bowen, H. K., Densification of alumina-silicon carbide powder composites: I. effects of a polymer coating on silicon carbide particles. *J. Am. Ceram. Soc.*, 1989, **72**, 948–953.
42. Xu, Y, Nakahira, A. and Niihara, K., Characteristics of Al_2O_3–SiC nanocomposite prepared by sol–gel processing. *J. Ceram. Soc. Jpn*, 1994, **102**, 312–315.
43. Wohlfromm, H., Processing and properties of Al_2O_3/SiC-nanocomposites. In *Ceramic Transactions* **Vol. 51**, *Ceramic Processing and Science*, ed. H. Hausner, G. L. Messing and S.-I. Hirano. The American Ceramic Society, Westerville OH, 1995, pp. 659–663.
44. Timms, L., Razer, B. L., Pearce, D. H., Jickells, A. and Ponton, C. B., Processing, microstructure and high temperature behaviour of Al_2O_3/SiC nanocomposites. In *Fourth Euro. Ceramics Vol. 4*, ed. A. Bellosi. Gruppo Editoriale Faenza Editrice S.p.A., Faenza, 1995, pp. 37–44.
45. Jiao, S., Borsa, C. E. and Walker, C. N., The microstructures of alumina ceramics containing nanoparticles of silicon carbide or titanium nitride. *Silicates Industriels*, 1995, **1995/7-8**, 211–214.
46. Nieto, M. I., Miranzo, P., de Aza, S. and Moya, J. S., Effect of atmosphere on microstructural evolution of pressureless sintered Al_2O_3/SiC composites. *J. Ceram. Soc. Jpn*, 1992, **100**, 459–462.
47. Wang, J., Ponton, C. B. and Marquis, P. M., Thermal stability of Al_2O_3–5 vol% SiC nanocomposite. *J. Mater. Sci.*, 1995, **30**, 321–333.
48. Gadalla, A., Elmasry, M. and Kongkachuichay, P., High temperature reactions within SiC–Al_2O_3 composites. *J. Mater. Res.*, 1992, **7**, 2585–2592.
49. Misra, A. K., Thermochemical analysis of the silicon carbide– alumina reaction with reference to liquid-phase sintering of silicon carbide. *J. Am. Ceram. Soc.*, 1991, **74**, 345–351.
50. Borsa, C. E. and Brook, R. J., Fabrication of Al_2O_3/SiC nanocomposites using a polymeric precursor for SiC. In *Ceramic Transactions* **Vol. 51**, *Ceramic. Processing and Science*, ed. H. Hausner, G. L. Messing and S.-I. Hirano. The American Ceramic Society, Westerville OH, 1995, pp. 653–657.
51. Su, B. and Sternitzke, M., A novel processing route for alumina/SiC nanocomposites by Si-polymer pyrolysis. In *Fourth Euro. Ceramics Vol. 4*, ed. A. Bellosi. Gruppo Editoriale Faenza Editrice S.p.A., Faenza, 1995, pp. 109–116.
52. Sternitzke, M., Derby, B., Brook, R. J., Su, B. and Fan, Q., Al_2O_3/SiC nanocomposites by hybrid polymer and powder processing. In *Ceramic Engineering & Science Proceedings* **17**, 1996, in press.
53. Conder, R. J., Ponton, C. B. and Marquis P. M., Processing of alumina/silicon carbide nanocomposites. *Br. Ceram. Proc.*, 1993, **51**, 105–115.
54. Haaland, R. S., Lee, B. I. and Park, S. Y., SiC/Al_2O_3 gel-derived monolithic nanocomposites. *Ceram. Engng Sci. Proc.*, 1987, **8**, 879–885.
55. Zhao, J., Stearns, L. C., Harmer, M. P., Chan, H. M., Miller, G. A. and Cook, R. E., Mechanical behavior of alumina-silicon carbide nanocomposites *J. Am. Ceram. Soc.*, 1993, **76**, 503–510.
56. Nakahira, A. and Niihara, K., Microstructures and fracture behaviors at high temperatures for Al_2O_3–SiC nanocomposites. In *Fracture Mechanics of Ceramics*, Vol. **9**, ed. R. C. Bradt *et al.* Plenum Press, New York, 1992, pp. 165–178.
57. Hoffman, M. J., Sternitzke, M., Rödel, J. and Brook, R. J., Fracture mechanisms in a strengthened nano-toughened alumina/silicon carbide composite. In *Fracture Mechanics of Ceramics*, Vol. 12, eds R. C. Bradt, D. P. H. Hasselman, D. Munz, M. Sakai and V. Ya. Shevchenko, Plenum Press, New York, 1996, pp. 179–186.
58. Davidge, R. W., Brook, R. J., Cambier, F., Poorteman, M., Leriche, A., O'Sullivan, D., Hampshire, S. and Kennedy, T., Fabrication, properties and modelling of engineering ceramics reinforced with nanoparticles of silicon carbide. *J. Eur. Ceram. Soc.*, 1996, **16**, 799–802.
59. Davidge, R. W., Twigg, P. C. and Riley, F. L., Effects of silicon carbide nano-phase on the wet erosive wear of polycrystalline alumina. *J. Eur. Ceram. Soc.*, 1996, **16**, 799–802.
60. Thompson, A. M., Fang, J., Chan, H. M. and Harmer, M. P., High temperature behavior of Al_2O_3:SiC 'nanocomposites'. In *Ceramic Transactions* **Vol. 51**, *Ceramic Processing and Science*, ed. H. Hausner, G. L. Messing and S.-I. Hirano. The American Ceramic Society, Westerville OH, 1995, pp. 671–678.
61. Nakahira, A., Sekino, T., Suzuki, Y. and Niihara, K., High-temperature creep and deformation behaviour of Al_2O_3/SiC nanocomposites. *Ann. Chim. Fr.*, 1993, **18**, 403–408.
62. Ohji, T., Nakahira, A., Hirano, T. and Niihara, K., Tensile creep behavior of alumina/silicon carbide nanocomposite. *J. Am. Ceram. Soc.*, 1994, **77**, 3259–3262.

63. Ohji, T., Hirano, T., Nankahira, A. and Niihara, K., Particle/matrix interface and its role in creep inhibition in alumina/silicon carbide nanocomposites. *J. Am. Ceram. Soc.*, 1996, **79**, 33–45.
64. Greskovich, C. and Palm, J. A., Observations on the fracture toughness of β-Si_3N_4–β-SiC composites. *J. Am. Ceram. Soc.*, 1980, **63**, 597–599.
65. Sasaki, G., Nakase, H., Suganuma, K., Fujita, T. and Niihara, K., Mechanical properties and microstructure of Si_3N_4 matrix composite with nano-metre scale SiC particles. *J Ceram. Soc. Jpn*, 1992, **100**, 536–540.
66. Hirano, T. and Niihara, K., Microstructure and mechanical properties of Si_3N_4/SiC composites. *Mater. Lett.*, 1995, **22**, 249–254.
67. Sasaki, G., Suga, T., Suganuma, K., Fujita, T. and Niihara, K., Sintering behavior of Si_3N_4 matrix composite with nano-metre SiC particles. In *Trans. of the Mater. Res. Soc. Jpn*, 1994, **16B**, 1517–1520.
68. Hirano, T., Nakahira, A. and Niihara, K., Effect of SiC particles on α-β Phase transformation and mechanical properties of Si_3N_4/SiC composites. *J. Japan Soc. Powder Powder Metall.*, 1994, **41**, 1243–1248.
69. Akimune, Y., Ogasawara, T. and Hirosaki, N., Influence of starting powder characteristics on mechanical properties of SiC-particle/Si_3N_4 composites. *J. Ceram. Soc. Jpn*, 1992, **100**, 463–467.
70. Akimune, Y., Hirosaki, N. and Ogasawara, T., Mechanical properties and microstructure in sintered and HIPed SiC particle/Si_3N_4 composites. *J Mater. Sci.*, 1992, **27**, 6017–6021.
71. Ishizaki, K. and Yanai, T., Si_3N_4 grain boundary reinforcement by SiC nanocomposites. *Silicates Industriales*, 1995, **1995/7-8**, 215–222.
72. Lee, S. Y., Park, D. S., Kim, S., Kim, H. D., Lee, H. S. and Kang J. B., The fabrication of Si_3N_4/SiC nano-composites. *Trans. Mater. Res. Soc. Jpn*, 1994, **Vol. 14A**, 899–902.
73. Kaiser, A., Vaßen, R., Stöver, D., Buchkremer, H. P. and Kesternich, W., Composites of Si_3N_4 and nanosized SiC. *Silicates Industriels*, 1996, **1996/5-6**, 111–115.
74. Suzuki, T., Kawakami, T., Koyama, T., Izaki, K., Nakano, R., Shitara, T., Hakkei, K., Hirani, T. and Niihara, K., Preparation of fine silicon nitride powders by vapor phase reaction of nitrogen-containing organosilicon compound with ammonia. *J. Ceram. Soc. Jpn, Int. Edn*, 1987, **95**, 75–79.
75. Niihara, K., Suganuma, K., Nakahira, A. and Izaki K., Interfaces in Si_3N_4–SiC nanocomposite. *J. Mater. Sci. Lett.*, 1990, **9**, 598–599.
76. Niihara, K., Hirano, T., Nakahira, A,, Ojima, K., Izaki, K. and Kawakami, T., High-temperature performance of Si_3N_4–SiC composites from fine amorphous Si–C–N powder. In *Proc. of MRS Int. Meet. on Advanced Materials*, 1989, Vol. **5**, 107–112.
77. Niihara, K., Hirano, T., Nakahira, A., Suganuma, K., Izaki, K. and Kawakami, T., Nanostructure and thermomechanical properties of Si_3N_4/SiC composites fabricated from Si–C–N precursor powders. *J. Japan Soc. Powder Powder Metall.*, 1989, **36**, 243–247.
78. Niihara, K., Izaki, K. and Kawakami, T., Hot-pressed Si_3N_4–32% SiC nanocomposite from amorphous Si–C–N powder with improved strength above 1200°C. *J. Mater. Sci. Lett.*, 1990, **10**, 112–114.
79. Niihara, K., Hirano, T., Nakahira, A. and Izaki, K., The correlation between interface structure and mechanical properties for silicon nitride based nanocomposites. In *Grain Boundary Controlled Properties of Fine Ceramics*, ed. K. Ishizaki, K. Niihara, M. Isotani and R. G. Ford. Elsevier Applied Science, London, 1992, pp. 103–111.
80. Riedel, R., Strecker, K. and Petzow, G., In-situ polysilane-derived silicon carbide particulates dispersed in silicon nitride composite. *J. Am. Ceram. Soc.*, 1989, **72**, 2071–2077.
81. Riedel, R., Seher, M. and Becker, G., Sintering of amorphous polymer-derived Si, N and C containing composite powders. *J. Eur. Ceram. Soc.*, 1989, **5**, 113–122.
82. Riedel, R., Seher, M., Mayer, J. and Szabó, D. V., Polymer-derived Si-based bulk ceramics, part I: Preparation, processing and properties. *J. Eur. Ceram. Soc.*, 1995, **15**, 703–715.
83. Mayer, J., Szabó, D. V., Rühle, M., Seher, M. and Riedel, R., Polymer-derived Si-based bulk ceramics, part II: Microstructural characterisation by electron spectroscopic imaging. *J. Eur. Ceram. Soc.*, 1995, **15**, 717–727.
84. Sawagushi, A., Toda, K. and Niihara, K., Mechanical and electrical properties of silicon nitride–silicon carbide nanocomposite material. *J. Am. Ceram. Soc.*, 1991, **74**, 1142–1144.
85. Messier, D. R., Riley, F. L. and Brook, R. J., The α/β silicon nitride phase transformation. *J. Mater. Sci.*, 1978, **13**, 199–1205.
86. Pan. Q. X., Mayer, J., Rühle, M. and Niihara, K., Silicon-nitride based ceramic nanocomposites. *J. Am. Ceram. Soc.*, 1996, **79**, 585–590.
87. Rendtel, A., Hübner, H. and Herrmann, M., Creep behaviour of Si_3N_4/SiC-nanocomposite materials. In *Fourth Euro. Ceramics Vol. 4*, ed. A. Bellosi. Gruppo Editoriale Faenza Editrice S.p.A., Faenza, 1995, pp. 225–232.
88. Pezzotti, G. and Sakai, M., Effect of a silicon carbide nano-dispersion on the mechanical properties of silicon nitride. *J. Am. Ceram. Soc.*, 1994, **77**, 3039–3041.
89. Yasuda, E., Bao, Q. and Niihara, K., The effects of fine SiC particles on the creep of MgO at high temperatures. *J. Ceram. Soc. Jpn*, 1992, **100**, 514–519.
90. Takada, H., Nakahira, A., Ohnishi, H., Ueda, S. and Niihara, K., Improvement of mechanical properties of natural mullite/SiC nanocomposites. *J. Japan Soc. Powder Powder Metall.*, 1991, **38**, 348–351.
91. Sakka, Y., Bidinger, D. D. and Aksay, A., Processing of silicon carbide-mullite-alumina nanocomposites. *J. Am. Ceram. Soc.*, 1995, **78**, 479–486.
92. Ge, Q. L., Lei, T. C. and Zhou, Y., Microstructure and mechanical properties of hot pressed Al_2O_3–ZrO_2 ceramics prepared from ultrafine powders. *Mater. Sci. Tech.*, 1991, **7**, 490–494.
93. Niihara, K., Zeng, J., Nakahira, A., Sekino, T., Miyamoto, Y., Ohnishi, H. and Kawanami, T., HIPing effects for ZrO_2 strengthened Al_2O_3 based nanocomposites. In *Hot Isostatic Pressing. Theory and Applications*, ed. M. Koizumi. Elsevier Applied Science, London, 1992, pp. 413–418.
94. Niihara, K., Ünal, N. and Nakahira, K., Mechanical properties of (Y-TZP)-alumina-silicon carbide nanocomposites and the phase stability of Y-TZP particles in it. *J. Mater. Sci.*, 1994, **29**, 164–168.
95. Nawa, M., Sekino, T. and Niihara, K., Fabrication and mechanical behaviour of Al_2O_3/Mo nanocomposites. *J. Mater. Sci.*, 1994, **29**, 3185–3192.
96. Sekino, T., Nakahira, A. and Niihara, K., Relationship between microstructure and high-temperature mechanical properties for Al_2O_3/W nanocomposites. In *Trans. Mater. Res. Soc. of Jpn*, 1994, **16B**, pp. 1513–1516.
97. Iwata, M., Nakahira, A., Inada, H. and Niihara, K., Fiber-reinforced Sialon/SiC nanocomposites with highly improved toughness and strength. In *Trans. Mater. Res. Soc. Jpn*, 1994, **16B**, pp. 1533–1536.
98. Kanamaru, M., Tatsuno, T. and Kusaka, T., Hot-pressed Al_2O_3/SiC whisker/TiC nano-composites. *J. Ceram. Soc. Jpn*, 1992, **100**, 408–412.
99. Jang, B.-K. and Kishi, T., Fabrication and microstructure of Al_2O_3–SiC–YAG hybrid composites prepared by particulate dispersion. *J. Am. Ceram. Soc.*, 1994, **77**, 1375–1376.
100. Liu, D.-M. and Fu, C.-T., Heat conduction of composites and its dependence on the microstructure of Al_2O_3–Cr_3O_2 composite. *Acta Metall. Mater.*, 1995, **43**, 1001–1006.

101. Chae, K.-W., Kim, D.-Y. and Niihara, K., Sintering of Al_2O_3–TiC composite in the presence of liquid phase. *J. Am. Ceram. Soc.*, 1995, **78**, 257–259.
102. Pacheco-Malagon, G., Garcia-Borquez, A., Coster, D., Sklyarov, A., Petit, S. and Fripiat, J. J., TiO_2–Al_2O_3 nanocomposites. *J. Mater. Res.*, 1995,**10**, 1264–1269.
103. Suzuki, Y., Sekino, T. and Niihara, K., Effects of ZrO_2 addition on microstructure and mechanical properties of $MoSi_2$. *Scripta Metall. Mater.*, 1995, **33**, 69–74.
104. Sasaki, G., Suga, T., Yanai, T., Suganuma, K. and Niihara, K., Microstructure of B_4C/TiB_2 composite fabricated by reaction sintering of B_4C and TiC. *J. Ceram. Soc. Jpn*, 1994, **102**, 321–325.
105. Su, K., Nowakowski, M., Bonnell, D. and Sneddon, L. G., Polymer precursor route to TiB_2/TiN nanocomposites. *Chem. Mater.*, 1992, **4**, 1139–1141.
106. Yamagishi, C., Tsukamoto, K., Hakoshima, J., Shimojima, H. and Akiyama, Y., Mechanical properties and microstructure of β-SiAlON–β–SiC composites by pressureless sintering. *J. Mater. Sci.*, 1992, **27**, 1908–1912.
107. Smith, C. S., Grains, phases and interphases: An interpretation of the microstructure. *Trans Metall. Soc., AIME*, 1949, **175**, 15–51.
108. Lange, F. F., Davis, B. I. and Askay, I. A., Processing-related fracture origins: III, differential sintering of ZrO_2 agglomerates in Al_2O_3/ZrO_2 composite. *J. Am. Ceram. Soc.*, 1983, **66**, 407–408.
109. Thompson, A. M., Chan, H. M., Harmer, M. P. and Cook, R. F., Crack healing and stress relaxation in Al_2O_3–SiC nanocomposites. *J. Am. Ceram. Soc.*, 1995, **78**, 567–571.
110. Fang, J., Chan, H. M. and Harmer, M. P., Residual stress relaxation behaviour in Al_2O_3–SiC nanocomposite. *Mater. Sci. Engng*, 1995, **A195**, 163–167.
111. Lawn, B., *Fracture of Brittle Solids*. Cambridge University Press, Cambridge, 1993.
112. Davidge, R. W. and Green, T. J., The strength of two-phase ceramic/glass materials. *J. Mater. Sci.*, 1968, **3**, 629–634.
113. Faber, K. T. and Evans, A. G., Crack deflection process — I. theory; *Acta Metall.*, 1983, **31**, 565–576.
114. Jiao, S., Jenkins, M. L. and Davidge, R. W., Interfacial fracture energy – mechanical behaviour relationship Al_2O_3/SiC and Al_2O_3/TiN nanocomposites. *Acta Metall. Mater.*, 1997, **45**, 149–156.
115. Jiao, S., Jenkins, M. L. and Davidge, R. W., Electron microscopy of crack/particle interactions in alumina/SiC nanocomposites. Presented at *Microscopy of Composites III, Oxford*, April 1996.
116. Green, D. J., Fracture toughness predictions for crack bowing in brittle particulate composites. *J. Am. Ceram. Soc.*, 1983, **66**, C4–C5.
117. Pezzotti, G., Nishida, T. and Sakai, M., Physical limitations of the inherent toughness and strength in ceramic-ceramic and ceramic-metal nanocomposites. *J. Ceram. Soc. Jpn*, 1995, **103**, 901–909.
118. Selsing, J., Internal stresses in ceramics. *J. Am. Ceram. Soc.*, 1961, **44**, 419.
119. Taya, M., Hayashi, S., Kobayashi, A. S. and Yoon, H. S., Toughening of a particulate-reinforced ceramic-matrix composite by thermal residual stress. *J. Am. Ceram. Soc.*, 1990, **73**, 1382–1391.
120. Levin, I., Kaplan, W. D., Brandon, D. G. and Wieder, T., Residual stresses in alumina–SiC nanocomposites. *Acta Metall. Mater.*, 1994, **42**, 1147–1154.
121. Todd, R. I., Bourke, M. A. M., Borsa, C. E. and Brook, R. J., Measurement and role of residual stresses in alumina/SiC nanocomposites. In *Fourth Euro. Ceramics Vol. 4*, ed. A. Bellosi. Gruppo Editoriale Faenza Editrice S.p.A., Faenza, 1995, pp. 217–224.
122. Pezzotti, G., Sergo, V., Ota, K., Sbaizero. O., Muraki, N., Nishida, T. and Sakai, M., Residual stresses and apparent strengthening in ceramic-matrix nanocomposites. *J. Ceram. Soc. Jpn*, 1996, **104**, 497–503.
123. Levin, I., Kaplan, W. D., Brandon, D. G. and Layyous, A. A., Effect of SiC submicrometer particle size and content on fracture toughness of alumina-SiC nanocomposites. *J. Am. Ceram. Soc.*, 1995, **78**, 254–256.